

INFORMATION TO USERS

This manuscript has been reproduced from the microfilm master. UMI films the text directly from the original or copy submitted. Thus, some thesis and dissertation copies are in typewriter face, while others may be from any type of computer printer.

The quality of this reproduction is dependent upon the quality of the copy submitted. Broken or indistinct print, colored or poor quality illustrations and photographs, print bleedthrough, substandard margins, and improper alignment can adversely affect reproduction.

In the unlikely event that the author did not send UMI a complete manuscript and there are missing pages, these will be noted. Also, if unauthorized copyright material had to be removed, a note will indicate the deletion.

Oversize materials (e.g., maps, drawings, charts) are reproduced by sectioning the original, beginning at the upper left-hand corner and continuing from left to right in equal sections with small overlaps.

Photographs included in the original manuscript have been reproduced xerographically in this copy. Higher quality 6" x 9" black and white photographic prints are available for any photographs or illustrations appearing in this copy for an additional charge. Contact UMI directly to order.

**ProQuest Information and Learning
300 North Zeeb Road, Ann Arbor, MI 48106-1346 USA
800-521-0600**

UMI[®]

NOTE TO USERS

This reproduction is the best copy available.

UMI

University of Alberta

***Engineering Molecular Architecture of Hydrophobically Modified
Poly(N-Isopropylacrylamide)***

by

Asif Mustafi Jalil



**A thesis submitted to the Faculty of Graduate Studies and Research in partial
fulfillment of the requirements for the degree of *Master of Science***

Department of *Biomedical Engineering*

Edmonton, Alberta

Spring 2002



**National Library
of Canada**

**Acquisitions and
Bibliographic Services**

395 Wellington Street
Ottawa ON K1A 0N4
Canada

**Bibliothèque nationale
du Canada**

**Acquisitions et
services bibliographiques**

395, rue Wellington
Ottawa ON K1A 0N4
Canada

Your file Votre référence

Our file Notre référence

The author has granted a non-exclusive licence allowing the National Library of Canada to reproduce, loan, distribute or sell copies of this thesis in microform, paper or electronic formats.

The author retains ownership of the copyright in this thesis. Neither the thesis nor substantial extracts from it may be printed or otherwise reproduced without the author's permission.

L'auteur a accordé une licence non exclusive permettant à la Bibliothèque nationale du Canada de reproduire, prêter, distribuer ou vendre des copies de cette thèse sous la forme de microfiche/film, de reproduction sur papier ou sur format électronique.

L'auteur conserve la propriété du droit d'auteur qui protège cette thèse. Ni la thèse ni des extraits substantiels de celle-ci ne doivent être imprimés ou autrement reproduits sans son autorisation.

0-612-69718-5

Canada

University of Alberta

Library Release Form

Name of Author: *Asif Mustafi Jalil*

Title of Thesis: *Engineering Molecular Architecture of Hydrophobically Modified Poly(N-Isopropylacrylamide)*

Degree: *Master of Science*

Year this Degree Granted: *2002*

Permission is hereby granted to the University of Alberta Library to reproduce single copies of this thesis and to lend or sell such copies for private, scholarly or scientific research purposes only.

The author reserves all other publication and other rights in association with the copyright in the thesis, and except as herein before provided, neither the thesis nor any substantial portion thereof may be printed or otherwise reproduced in any material form whatever without the author's prior written permission.



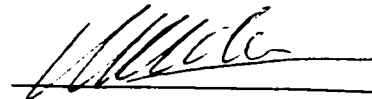
*417-8515-112 Street
Edmonton, Alberta
T6G 1K7
Canada*

Date: April 09, 2002

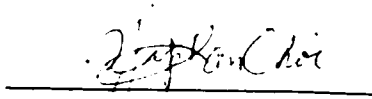
University of Alberta

Faculty of Graduate Studies and Research

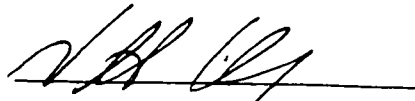
The undersigned certify that they have read, and recommend to the Faculty of Graduate Studies and Research for acceptance, a thesis entitled *Engineering Molecular Architecture of Hydrophobically Modified Poly(N-Isopropylacrylamide)* submitted by *Asif Mustafi Jalil* in partial fulfillment of the requirements for the degree of *Master of Science*.



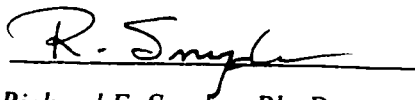
Hasan Uludag, Ph. D.
Department of Chemical and
Materials Engineering



Phillip Y. K. Choi, Ph. D.
Department of Chemical and
Materials Engineering



Jonathan Lakey, Ph. D.
Department of Surgery



Richard E. Snyder, Ph. D.
Department of Biomedical Engineering

Date: February 21, 2002

This thesis is dedicated to my wife, Ameena Hashmi, who supported me through out the whole process.

I would also like to thank my supervisor, Hasan Uludag, for his time and invaluable feedback.

I would also like to thank my colleagues, Sebastien Gittens, Erin Smith, and Jennifer Yang for their friendship.

ABSTRACT

This project was carried out to engineer protein reactive N-isopropylacrylamide (NiPAM) polymers using methylmethacrylate (MMA) to exhibit a controlled lower critical solution temperature (LCST) and to improve their gel stability. A methodology for comb-type polymer (CP) synthesis was first developed. The effect of polymer architecture and molecular weight on polymer's physical properties (i.e., LCST and gel stability) was then investigated. It was found that the LCST of CP remained unchanged as mol% MMA was increased. In contrast, LCST of random polymer (RP) decreased with increasing mol% of MMA. However, the gels of low molecular weight (MW) CPs were more stable than those of RPs. For both types of polymers, gel stability improved with increase in MW. Gel stability of CP was independent of MMA side chain length, which was between 3 and 10 kD. Protein reactive ends of these polymers were obtained by using free radical initiator with protein reactive succinimide ends during the thermal polymerization process. These end-functionalized polymers showed capacity to conjugate to the model protein, albumin. Overall, this thesis showed that the temperature sensitive polymer with controlled architecture could be engineered. In the future, these polymers will be useful in delivering immunosuppressive protein *in vivo*.

Table of Contents

1. General Introduction	1
2. Literature Review	3
2.1.Cell Encapsulation	3
2.2.Immunoregulatory Proteins	5
2.3.Temperature Sensitive Polymers	7
3. Thesis Approach	10
4. Materials and Method	11
4.1.Succinimide ester of V501 Synthesis (A501)	11
4.2.Poly-MMA (PMMA) Macromonomer Synthesis	12
4.3.Semitelechelic MMA Macromonomer Synthesis	15
4.4.MW Determination of Semitelechelic MMA-NH ₂	18
4.5.Synthesis of Random Polymer and Comb-Polymer	18
4.6.NiPAM and MMA Contents of the Polymer	21
4.7.Acrylic Acid Contents of the Polymer	22
4.8.Succinimide Contents of the Polymer	22
4.9.Weight-Average MW of the Polymer	23
4.10.LCST by Spectroscopy	24
4.11.NASI Aminolysis Rate	25
4.12.Degelation of Polymer Gels	26
4.13.BSA Conjugation to End-Functionalized Polymer	26
5. Results	27
5.1.Overall Approach	27
5.2.Phase I: MMA Macromonomer Synthesis	29
5.2.1. PMMA Macromonomer	29
5.2.2. Synthesis of Comb-Type Polymers	32
5.2.3. Synthesis of Macromonomer	33
5.3.Phase II: Synthesis and Characterization of CP and RP	36
5.3.1. Synthesis of Macromonomer	36

5.3.2. Comb-Type Polymers	38
5.3.3. Random Polymers	46
5.3.4. Degelation of Hydrogels	53
5.4. Protein Conjugation	65
5.4.1. BSA Conjugation to Polymer	65
6. Discussion	67
6.1. Free Radical Polymerization	67
6.2. N-Terminal Reactivity	69
6.3. CP vs. RP	72
7. Conclusions	76
8. Future Directions	77
9. Literature Cited	78
10. Appendices	84
10.1. A	86
10.2. B	87
10.3. C	88
10.4. D	89
10.5. E	90
10.6. F	91

List of Tables

1. Amount of MMA, AET, VA086, and DMF that were used to synthesize semitelechelic MMA.....	15
2. The amount of semitelechelic MMA-NH ₂ and acryloyl chloride that were used to synthesize semitelechelic MMA macromonomer.....	16
3. Amount of reactants that were used to synthesize RPs	19
4. Amount of reactants that were used to synthesize CPs with 72 kD MMA side chain	20
5. Amount of reactants that were used to synthesize CPs with 10 kD MMA side chain	20
6. Amount of reactants that were used to synthesize CPs with 6 kD MMA side chain	20
7. Amount of reactants that were used to synthesize CPs with 4 kD MMA side chain	21
8. Amount of reactants that were used to synthesize CPs with 3 kD MMA side chain	21
9. LCST and MWs of CP	32
10. MW of semitelechelic PMMA-NH ₂	33
11. MW of semitelechelic PMMA-NH ₂	36
12. Physical properties of CP (MW of MMA macromonomer: 10 kD)	39
13. Physical properties of CP (MW of MMA macromonomer: 6 kD)	39
14. Physical properties of CP (MW of MMA macromonomer: 3 kD)	39
15. Physical properties of RP	47
16. T ₅₀ of CP hydrogel	54
17. T ₅₀ of high MW RP hydrogel	54
18. Physical characteristics of RP and CP that were reacted with BSA	65
19. Titration of amino terminated (14 % AET) semitelechelic MMA	86
20. Amount of NaOH was added to neutralize AAc of a particular polymer	88
21. Raw data for CPI degelation study	91

List of Figures

1. A501 synthesis	13
2. PMMA macromonomer synthesis using amide condensation reaction	14
3. Semitelechelic PMMA macromonomer synthesis using telomerization and amide condensation reactions	17
4. The chemical shifts for NiPAM and MMA	22
5. Molecular architecture of RP and CP	28
6. PMMA-NHS aminolysis using ethylenediamine	30
7. NASI aminolysis as a function of PMMA-NH ₂	31
8. NASI aminolysis as a function of semitelechelic MMA-NH ₂	34
9. NMR spectrum of semitelechelic MMA macromonomer	35
10. MW of semitelechelic MMA-NH ₂ as a function of mol% AET	37
11. LCST of CPs as a function of AAc in CP	41
12. Low and high MW CP synthesized in dioxane and benzene	42
13. MMA composition of the synthesized CP	43
14. LCST of CPs as a function of MMA in CP	44
15. Succinimide concentration as a function of MW of CP	45
16. LCST of RPs as a function of observed mol% AAc	48
17. Low and high MW RP synthesized in dioxane and benzene	49
18. MMA composition of the synthesized RP	50
19. LCST of RP as a function of observed mol% MMA	51
20. Succinimide concentration as a function of MW of RP	52
21. High and low MW CP with 10 MMA side chain	55
22. High and low MW CP with 6 MMA side chain	56
23. High and low MW CP with 3 MMA side chain	57
24. High MW CP with different length of MMA side chain	58
25. Low MW CP with different length of MMA side chain	59
26. Low MW CP with different amount of MMA	60
27. High MW CP with different amount of MMA	61

28. High MW RP	62
29. T_{50} of CP hydrogels as a function of their LCST	63
30. T_{50} of CP hydrogels as a function of their MW	64
31. Protein conjugation	66
32. Trypsin conjugation to Poly NiPAM	71
33. A theoretical titration curve for amino terminated semitelechelic MMA	86
34. Succinimide Calibration Curve	89
35. LCST of NiPAM polymer that was synthesized in benzene	90
36. Hydrogel dissolution curve of CP1	91

List of Abbreviations

- A501 – 4,4'-azobis(4-cyanovalerate succinimide).
AAc – acrylic acid.
AcCl – acryloyl chloride.
AET – 2-aminoethanethiol.
B – Benzene.
CP – comb-type polymer.
D- 1,4, Dioxane.
DCC – 1,3-dicylohexylcarbodiimide.
MMA – methylmethacrylate.
MW – weight average molecular weight.
NASI – N-acryloxysuccinimide.
NHS – N-hydroxylsuccinimide.
NiPAM – N-isopropylacrylamide.
NMR – nuclear magnetic resonance.
PMMA – polymethylmethacrylate.
RP – random polymer.
V501 – 4,4'-azobis(4-cyanovaleric acid)
VA086 – 2,2'-Azobis[2-methyl-N-(2-hydroxyethyl)propionamide].

GENERAL INTRODUCTION

Transplantation of cells to treat variety of human diseases, such as hormone or protein deficiencies, is promising but problematic because of the immune rejection of the transplanted cells. Encapsulation of cells within polymeric membranes is a promising alternative method because it can protect the cells from immune attack by preventing the access of a host's immune system to the graft. Graft viability is retained since the capsule wall has minimal impediment to diffusion of small molecules, such as nutrients and metabolic end-products. Moreover, the capsules act as a permeability barrier to inflammatory cells, antibodies, and complement components. As a result, encapsulated cells retain their normal physiological state (e.g., Chinese Hamster Ovary fibroblasts) [Uludag and Sefton 1992; Uludag and Sefton 1993] and/or proliferate (e.g., hepatocytes) [Dixit et al. 1992] in addition to their ability to express differentiated functions (e.g., insulin secretion by the islets) [Calafiore et al. 1996; Tatakiewicz et al. 1994; Mikos et al. 1994; Garfinkel et al. 1998; Lum et al. 1991; Lum et al. 1992].

Long-term viability of the encapsulated cells, however, is compromised because of fibrotic overgrowth on the capsule membrane. The final outcome is necrosis due to impaired transmembrane gas/nutrient diffusion, and loss of ability to synthesize and secrete tissue or cell specific biomolecules. The reaction is directed against both capsule materials [Zekron et al. 1996] and graft antigens [Weber et al. 1990]. Although it is possible to improve capsule biocompatibility [Sawhney et al. 1993] or isolate biocompatible materials [Li 1997; Hunkler et al. 1997], reaction to graft antigens cannot be suppressed and continuously shed donor antigens can stimulate the immune system and lead to progressive build-up of a fibrous layer. In this respect, the survival of transplanted cells can be improved if the cells are transplanted in an "open" vascularized environment with no diffusion limitations. An immune regulatory mechanism can be incorporated into the "open" system by localizing immunosuppressive proteins at the graft site. Although, it is possible to engineer cells that express the immunoregulatory proteins at the graft site, such an approach is clinically challenging because of the need to isolate, culture, and transplant additional carrier cells. Hence, thermoreversible, protein-conjugating polymers are being explored as carriers for controlled delivery of therapeutic proteins [Uludag et al. 2000; Uludag and Fan 2000; Uludag et al. 2001]. Such polymers

can be designed so that they (i) can conjugate to proteins without crosslinking agents, (ii) are soluble at a low temperature (so that chemical manipulations can be carried out in a solution state), and (iii) are insoluble at the physiological temperature to form a gelled state at a site of application. In other words, the thermoreversible, protein-conjugating polymers can form an “open” gel system that provides the cells or tissues with the needed three-dimensional matrix while retaining immunoregulatory proteins to give protection from host’s immune system.

Immunoregulatory proteins that interact with cell surface receptors involved in initiation, progression, and down-regulation of an immune system are considered for this project. In specific, the ligand-receptor pair Fas and Fas Ligand (FasL) is considered. Fas and FasL are found at the immunoprivileged sites, such as eye [Griffith et al. 1995] and testis [Bellgrau et al. 1995] where they prevent graft rejection. Studies have elucidated that Fas protein (CD95) is ubiquitously expressed on a wide variety of cells whereas FasL is present mainly on natural killer and activated T-cells. Binding of FasL to Fas on T-cells results in apoptosis of T-cells, which can essentially shut down an immune response [Lowin et al. 1994; Strasser and O’Connor 1998]. Consequently, strategic FasL presence is proposed to protect transplanted cells from immune attack. FasL cannot be used for systematic immunosuppression due to its liver toxicity [Tanaka et al. 1997]. Local FasL delivery has been made feasible by engineering cells to express FasL [Lau et al. 1996] but such an approach is clinically challenging because of the need to isolate/culture/transplant an additional cell type. To avoid carrier cells, transplanted cells (e.g., pancreatic islets) were engineered by adenoviral infection and transgenic means but underwent apoptosis upon transplantation [Kang et al. 1997]. Because of this challenges, protein-conjugating polymers (e.g., NiPAM polymers with succinimide esters) are viable alternative for localizing FasL. Localized immunosuppression also avoids the adverse side effects (e.g., edema, opportunistic infections, metastatic lymphomas, etc.) of systematic immunosuppression.

In brief, the goal is to devise a blue print for tissue transplantation, which uses an “open” vehicle with immunoregulatory ability. In the future, the protein/polymer/tissue complex can be used to transplant pancreatic islets to treat diabetes, neural cells to treat Parkinson’s, hepatocytes to treat liver failure, and so on.

LITERATURE REVIEW

Two lines of research have provided preliminary data for the feasibility of cell transplantation without systemic drugs. One involves the transplantation of polymer-encapsulated cells, and the other implantation of immunosuppressive proteins with the grafts. Another line of research on thermoreversible polymer has shown the feasibility of devising an “open” gel system.

Cell Encapsulation

Mammalian cell encapsulation within physical membranes has been practiced for over four decades. The method has been developed based on the promise of its therapeutic usefulness in tissue transplantation. Recently, Uludag et al. have done a comprehensive, authoritative review of the technology behind the cell encapsulation [2000]. According to the review, encapsulation physically isolates a cell mass from an outside environment and aims to maintain normal cellular physiology within a desired permeability barrier. Numerous encapsulation techniques have been developed over the years. These techniques are generally classified as microencapsulation (involving small spherical vehicles and conformally coated tissues) and macroencapsulation (involving larger flat-sheet and hollow-fiber membranes). Microencapsulation techniques involve polyelectrolyte complexation, thermoreversible gelation, interfacial precipitation, interfacial polymerization, and so on. Macroencapsulation techniques involve flat sheet and hollow fiber-based technologies.

The challenges of cell encapsulation are to maintain cell viability during capsule formulation process and cell functions for an extended period of time. The requirement of the formulation process is that it has to take the fragile nature of the mammalian cells into account while forming uniform microcapsules. In other words, it is imperative that the exposure of cells to physical forces (e.g., shear, pressure, or osmosis) and toxic chemicals (e.g., polymer solvents) are minimized during the formulation process. Present microencapsulation techniques do these successfully. Lim and Sun, for example, demonstrated feasibility of encapsulating sensitive mammalian tissues using the polyelectrolyte complexation method (1980). The ionic

interactions that lead to capsule formation are entropy driven and that generate little or no heat; therefore, the formulation process is very gentle to the tissues. The biomaterials are nontoxic, and they form microbeads easily through a gentle process (i.e., minimum shear, pressure, or osmosis). Another microencapsulation technique so called interfacial precipitation method uses organic solvents to dissolve the polymers. However, by carefully controlling the pH, temperature, osmotic pressure, and solvent/reagent exposure, researchers are able to preserve cell viability during such an approach. For example, formation of polyacrylate microrcapsule utilizing interfacial precipitation was shown to maintain the viability of Chinese hamster ovary fibroblasts (CHO) [Uludag and Sefton 1992] and human hepatoma (HepG2) cells [Uludag and Sefton 1993].

In the long run, survival of the encapsulated cells depends on the following capsule properties: biocompatibility, size, microenvironmental conditions within the core, and mechanical stability. Polymeric materials that are biocompatible are important because poor biocompatibility often leads to fibrotic growth on the capsule membrane, which eventually chokes off transport to and from the encapsulated cells. The final outcome is loss of long-term cell viability: necrosis due to impaired transmembrane gas/nutrient diffusion, and loss of ability to synthesize and secrete tissue specific biomolecules. Alginate-polylysine capsules, for example, elicit inflammatory response due to poor biocompatibility of the alginate (Schilfgaarde and Vos 1998). Biocompatibility of alginate-polylysine capsules has been improved with moderate success by purifying alginate, by coating capsules with poly(ethylene glycol), and by incorporating monomethoxy poly(ethylene glycol) pendent chains to the polylysine polymer backbone. In addition, numerous other biomaterials (e.g., hydroxyethyl methacrylate-methyl methacrylate, polyphosphazene, agarose, etc.) have been studied using various encapsulation methods (e.g., coacervation, interfacial precipitation, etc.) to improve biocompatibility of the biomaterials [Li 1998; Hunkler et al. 1997]. However, as it was pointed out in the introduction, it is possible to improve capsule biocompatibility but reaction to graft antigens cannot be suppressed. This will stimulate the immune system and lead to progressive build-up of a fibrous layer. The

survival of the transplanted tissue can therefore be improved if the tissues are transplanted in an “open” vascularized environment with no diffusion limitations and with localized immunosuppressive proteins.

Immunoregulatory Proteins

Currently, a major drawback in performing organ or tissue transplantation is the toxic side effects of systemic immunosuppressants [Balow et al. 2000; de Mattos et al. 2000]. Localized delivery of immunosuppressive molecules to the hyperactive immune site could theoretically ameliorate many of the hazardous effects of immunosuppressive agents on unrelated tissues, as well as avoid systemic immunosuppression that leaves the recipient vulnerable to infectious agents. Implantation of immunosuppressive proteins such as, FasL, with the grafts and controlling the proteins' delivery offers a way of reducing the toxic side effects of immunosuppressants.

Testicular sertoli cells are known to constitutively express FasL. Therefore, cotransplantation of sertoli cells with grafts provides a way of localizing FasL. Takeda and coworkers cotransplanted allogenic islets with testicular tissue in streptozotocin-induced diabetic mice [1998]. They found that the islet/testicular composite ($>1 \times 10^3$ sertoli cells/islet) survived 17.5 days (mean survival time). In another study, Korbitt and colleagues found that all (5 of 5) streptozotocin-diabetic rats were normoglycemic at 95 days after receiving a composite graft of allogenic islets and sertoli cells [1997]. However, in mice with autoimmune diabetes, sertoli cells exerted FasL dependent neutrophil infiltration and graft destruction, which was opposed by immunosuppressive proteins IGF-I and TGF β from sertoli cells [Korbitt et al. 2000].

Since FasL is believed to mediate immune privilege and immunological tolerance [Abbas 1996], transgenic mice were used to express murine FasL on islet β cells [Allison et al. 1997] or on cardiomyocytes [Takeuchi et al. 1999]. Paradoxically, FasL expressing islets or heart grafts underwent accelerated neutrophilic rejection upon transplantation, which suggests a pro-inflammatory function of FasL in addition of its protective function. It is likely that the FasL on the islet cells of the transgenic mice stimulated IL-8 secretion by the neighboring Fas, which attracted the neutrophils

[Allison et al. 1997]. Chen and coworkers suggested that the destructive neutrophils can be blocked by coexpressing TGF- β with FasL [1998]. Another theory is that the Fas expression was up regulated on transgenic islets, which then interacted with the coexpressed FasL and underwent apoptosis [Allison et al. 1997]. It is suggested that the thyroid follicular cells (TFC) are resistant to Fas-mediated cell death because they express antiapoptotic proteins. Hence, in contrast to the abrogation of ectopic FasL expressive transgenic islets or cardiomyocytes, “dose dependent” transgenic expression of FasL on TFC prevented experimental autoimmune thyroiditis in mice [Batteux et al. 2000].

Also, nonviral vectors can be used to engineer grafts, so they express FasL. In a recent study, Batteux and colleague had injected a plasmid DNA that had code for FasL in the TFCs of mice [1999]. In so doing, they were able to express FasL on TFC for more than 15 days and prevented experimental autoimmune thyroiditis. To avoid carrier cells, FasL was also expressed on grafts by adenovirus infection. Although, systemic adenovirus mediated FasL (Ad.FasL) gene delivery induces massive hepatic failure *in vivo*, the strategy can be used to treat rheumatoid arthritis because peri or intra-articular injection of Ad.FasL localizes FasL expression inside the inflamed joints. Consequently, some groups were able to express FasL in the inflamed joints for minimum of 10 days and induce significant apoptosis of synovial fibroblasts without damaging the articular chondrocytes [Zhang et al. 1997; Yao et al. 2000]. Since, systemic recombinant adenovirus medicated FasL delivery induces massive hepatic injury *in vivo*, two research groups [Kang et al. 1997; Judge et al. 1998] have used adenovirus to deliver murine FasL cDNA to *ex vivo* pancreatic islets. However, the results following the transplantation of the islets were same as with the transgenic animals. This finding confers with the evidence that the ectopic expression of FasL stimulates an inflammatory response and targets the FasL-expressing tissue for destruction. So, to overcome the problem, FasL has been expressed within the local environment of allografts with the hope that the FasL will induce apoptosis of infiltrating T cells. Lau and colleagues investigated whether transplanting a composite graft, consisting of syngeneic FasL expressing myoblasts that was transfected using

calcium phosphate precipitation method, would protect the islet allografts from rejection [1996]. They found that FasL-transfected myoblasts protected the islets in a dose-dependent manner such that, in the group receiving the highest dose of myoblasts (2×10^6), three of eight grafts survived indefinitely (mean survival time >84.1 days). These results make FasL a potential immunosuppressant provided that the protein is delivered locally.

Temperature Sensitive Polymers

Thermoreversible or temperature sensitive polymers are considered “intelligent” polymers because they respond with large property changes to small physical or chemical stimuli. Recently, they have been engineered to have protein reactive groups, so they can act as a carrier for therapeutic proteins [Uludag et al. 2001] or conjugate to enzymes or receptor proteins [Hoffman et al. 2000]. According to Uludag et al., thermoreversible, protein-reactive polymers have attracted attention because the thermoreversible (i.e., temperature dependent solubility) characters of the polymers allow one to carry out desired manipulations, such as mixing, injecting, and protein conjugation, in a solution state but eventually enable one to induce a phase-separation simply by increasing the temperature above the solubility limit of the polymers [2001]. The fact that such a phase separation is driven only by a temperature change is attractive because no other exogenous molecules need to be added in a pharmaceutical dosage form. The protein reactivity of the polymers allows one to conjugate proteins to polymers without crosslinking agent; hence, the probability of altering the protein structure is reduced. Not surprisingly, these polymers are widely implemented in Medicine and biotechnology industry. For example, temperature-sensitive polymers are used to encapsulate mammalian cells [Vernon 1996], deliver bone morphogenic proteins to bone [Uludag et al. 2001], and in enzyme immobilization [Ding et al. 1998].

Polymers of N-isopropylacrylamide (NiPAM) have been the most commonly studied thermoreversible polymer. A NiPAM homopolymer exhibits a lower critical solution temperature (LCST) of 30-32 °C in water [Schild 1991]. It has been proposed

that the mechanism for LCST behavior is as follows [Schild and Tirrell 1990; Schild 1991]. At low temperatures, strong H-bonding between the lone electron pair on the nitrogens of NiPAM and hydrogens of water outweighs the unfavorable free energy related to exposure of hydrophobic groups to water. As the solution temperature increases, H-bonding weakens, while hydrophobic interactions between hydrophobic side groups increase. Above LCST, the interactions between hydrophobic groups become dominant and leads to an entropy-driven polymer collapse and phase separation. The reduced freedom of the polymer chain is compensated by the increase in entropy due to the release of structured water around the hydrophobic groups on the polymer. Supporting evidence for this model has been given by the differential scanning calorimetry (DSC) experiments, which show endothermic phase separation [Otake et al. 1990] in case of thermoreversible polymers. Moreover, Feil and coworkers found that in randomly distributed charged residues typically increased the LCST whereas hydrophobic residues lowered the LCST because the comonomers changed the overall hydrophilicity of NiPAM polymer [1993].

Research also shows that the molecular architecture of NiPAM copolymer influences the physical properties of the polymer. In case of hydrophobically modified random NiPAM copolymer, LCST decreases with the increase in hydrophobic monomer content [Feil et. al. 1993; Uludag and Fan 2000; Uludag et. al. 2001]. At fixed hydrophobic monomer content, LCST of NiPAM polymer decreases as the length of monomer chain increases [Uludag et. al 2001]. However, this relationship does not hold for NiPAM copolymers with longer ($> C_{18}$) hydrophobic side chains. Even though, researchers [Badiger et. al. 1998; Chung et. al. 1998] had observed an inverse linear relationship between the length of alkyl side group and the LCST of NiPAM copolymer, the length of hydrophobic side chain in their study was $< C_{18}$. In contrast, Ringsdorf and coworkers observed that for longer ($> C_{18}$) hydrophobic side chain, LCST of NiPAM copolymer remained unchanged [1991]. Using pyrene probe, they elucidated that the longer alkyl chains were not exposed to water but rather formed a micellar structure protected from the water and therefore do not make hydrophobic contribution. Using fluorescence technique, Ringsdorf and coworkers also found that

the micelles were severely disrupted above LCST [1992]. The original hydrophobic core was destroyed and the hydrophobic groups became entangled within the polymer rich phase. Chung and coworkers [1998] observed that the micellar size of NiPAM polymer with hydrophobic side chain increased after heating/recooling cycles. This shows that the structure of the single modified NiPAM chain influences the supramolecular assembly or resiliency of the polymer gel.

For this project, we chose N-isopropylacrylamide (NiPAM) because of its thermoreversibility. The hydrated polymer collapses to a globular state above LCST to form micellar structures. Charged residues typically increase the LCST whereas hydrophobic residues lower the LCST [Feil et. al. 1993]. For this project, methylmethacrylate (MMA), a hydrophobic monomer, is used to lower the LCST below the physiological temperature. This is critical for gel resiliency, but not the only requirement for the polymers to form a gel *in vivo*. It is also essential that the induced polymeric micelles exhibit sufficient self-association for gelation. Therefore, to improve the micelle aggregation, we engineered the architecture of the NiPAM-MMA copolymer. Ringsdorf et al. showed that the micelle aggregation could be enhanced by separating and lengthening the hydrophobic chains of the NiPAM copolymer [1991]. Hence, we synthesized comb-type polymers by separating MMA from NiPAM backbone. Also, to investigate the effects of the polymer architecture on the polymer's physical properties such as, LCST and gel stability, we compared the physical properties of comb-type polymer with that of random NiPAM-MMA copolymer.

THESIS APPROACH

The goal of this project was to devise a blue print for tissue transplantation, which uses an “open” vehicle with immunoregulatory ability. The “open” vehicle is a hydrated polymeric gel, which is designed to hold the transplant tissue. Due to time constraint, only the “open” vehicle was engineered. Because of NiPAM’s thermoreversible property, the “open” vehicle was prepared using NiPAM polymer. The NiPAM polymers were engineered using MMA to exhibit a controlled LCST and improve hydrogel stability. The research for the thesis was carried out in two phases. In Phase I, a methodology for preparing end-functionalized semitelechelic MMA macromonomer was developed. In Phase II, comb-type polymers (CPs) were synthesized using the semitelomeric MMA macromonomer. The LCST and hydrogel stability of CPs were studied and compared to the LCST and hydrogel stability of random polymers (RPs). The conjugation reaction between bovine serum albumin (BSA) and the synthesized polymers was also investigated. To minimize altering the protein’s bioactivity, the polymers were synthesized to have protein reactive sites at the ends, instead of along the polymer backbone. The end functionalized polymers were obtained by preparing the Succinimide ester of an azo initiator 4,4’-Azobis(4-cyanovaleric acid). Succinimide esters were incorporated into the polymers to allow conjugation with amine groups, a side group common in proteins [Uludag and Fan 2000]. The reaction of end-group succinimide ester with an amine is expected to proceed with a mechanism similar to reaction of succinimide esters of small molecules. The latter is well studied and involves a nucleophilic attack at the carbonyl group adjacent to succinimide ring [Cline and Hanna 1988]. The end-group succinimide ester is also expected to lower the steric resistance for conjugation and cause minimal disruption to protein structure.

MATERIALS AND METHODS

Materials

Monoacid sodium phosphate was from Anachemia (Montreal, QC). Diethyl ether and chloroform were from Caledon Laboratories (Georgetown, ON). 4,4'-Azobis(4-cyanovaleric acid) or V501 and 2,2'-Azobis[2-methyl-N-(2-hydroxyethyl)propionamide] or VA086 were from Wako Chemicals (Richmond, VA). NiPAM, MMA, N-hydroxysuccinimide (NHS), 1,4-dioxane, anhydrous *N,N*-dimethylformamide (DMF), 2-methyl-2-propanol (t-butanol), ethylenediamine, anhydrous *N,N*-dimethylacetamide (DMA), 2-aminoethanethiol (AET), 1,3-dicyclohexylcarbodiimide (DCC), acrylic acid (AAc), benzene, and acryloyl chloride were from ALDRICH (Milwaukee, WI). Acetonitrile and methanol were from EM Science (Germany). Disodium hydrogen orthophosphate and perchloric acid were from BDH Chemicals (Toronto, ON). Acetic acid was from Fisher Scientific (Nepean, ON). The nuclear magnetic resonance (NMR) solvent deuterated chloroform (CDCl_3) was from Cambridge Isotope Laboratories (Andover, MA). The molecular weight (MW) standards were polystyrene of 44.0 kDa ($M_w/M_n = 1.07$) and 13.7 kD ($M_w/M_n = 1.01$). They were from ALDRICH. N-acryloxysuccinimide (NASI) was synthesized by acryloylchloride reaction with NHS in chloroform in the presence of triethylamine, as described in [Uludag et al. 2000]. The inhibitors in NiPAM, MMA, and AAc were removed by recrystallizing from n-hexane, through vacuum distillation, and by using ALDRICH inhibitor removal column, respectively.

Succinimide ester of V501 Synthesis (A501)

A501 was synthesized according to [Yang et al. 2000]. Briefly, V501 (3 g, 10.7 mmol) and NHS (2.5 g, 21 mmol) were dissolved in anhydrous DMF and then DCC (5.3 g, 26 mmol) was added to this solution. The reaction mixture was stirred at room temperature overnight. The solution was filtered to remove the precipitated dicyclohexylurea salt (by product), and A501 was obtained by precipitation in diethyl ether. The precipitant was recovered by filtration and dried under vacuum.

The described reaction scheme involves ester formation between the V501 carboxylic acid ends and NHS alcohol groups. These two functional groups react to form an ester bond. The role of DCC was interpreted from a similar reaction as described in [PIERCE handbook]. The reaction scheme is outlined in Figure 1. DCC reacts with the carboxylic groups of V501 to form an active O-acylisourea intermediate. This intermediate reacts with NHS to form the ester derivative of V501 and releases an insoluble urea salt.

Poly-MMA (PMMA) Macromonomer Synthesis

Following two types of macromonomers were synthesized for this project: PMMA macromonomer and semitelechelic MMA macromonomer. These two macromonomers differ in MW, the former being larger in size.

All glassware was washed with soap, distilled water, and acetone and baked under vacuum overnight. The glasswares were assembled under nitrogen after cooling. PMMA macromonomer was synthesized as outlined in Figure 2. The reaction conditions were as follow: MMA (20 g, 199.8 mmol) and 0.07 mol% A501 (0.0706 g, 0.15 mmol) were dissolved in 210 ml dioxane; the solution was purged with N₂ for 15 minutes; the polymerization was carried out at 80 °C for 24 hours, and the succinimide terminated MMA polymer (PMMA-NHS) was precipitated in diethyl ether, filtered and dried under vacuum. Yield: 11.9 g, 60%.

The step 2 of Figure 2 involves nucleophilic reaction between ethylenediamine and the succinimide end group of MMA polymer. The reaction generates an amide bond at the end of MMA polymer. Since, ethylenediamine has two amines, we used excess ethylenediamine to obtain partial reaction, which converted the succinimide end group to amine end group. For this project, PMMA-NHS (0.5 g, 0.007 mmol) and ethylenediamine (0.003g, 0.05 mmol) were added to 50 mL acetonitrile. It was assumed that PMMA-NHS had 0.1 mol % NHS, so 10 fold ethylenediamine was added. The reaction mixture was stirred at room temperature for 24 hours, and then PMMA-NH₂ was precipitated in MeOH and dried under vacuum.

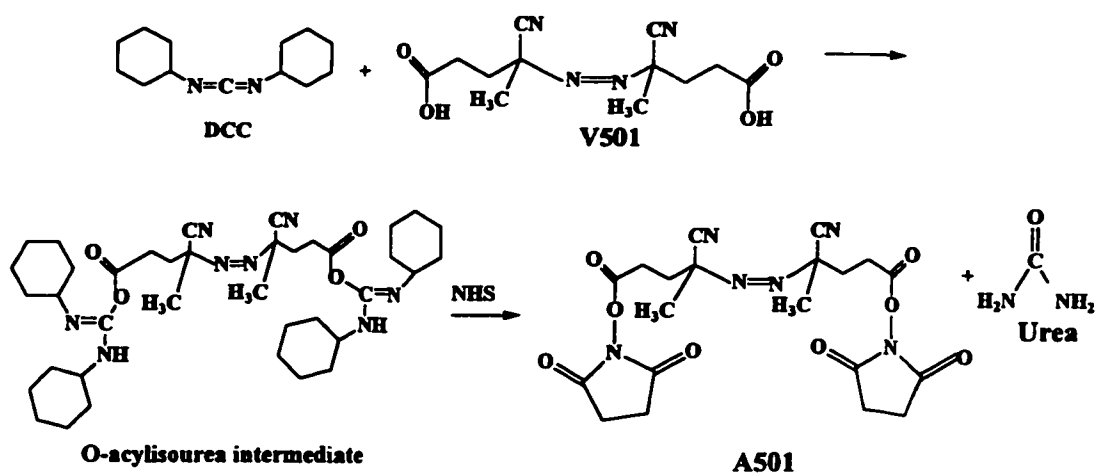


Figure 1. A501 synthesis. In the first step, DCC reacts with the carboxylic acid group of V501, which activates the carboxylic group, allowing it to be coupled to the NHS in the reaction mixture. In the second step, DCC is released as a soluble urea derivative after displacement by the nucleophilic, NHS.

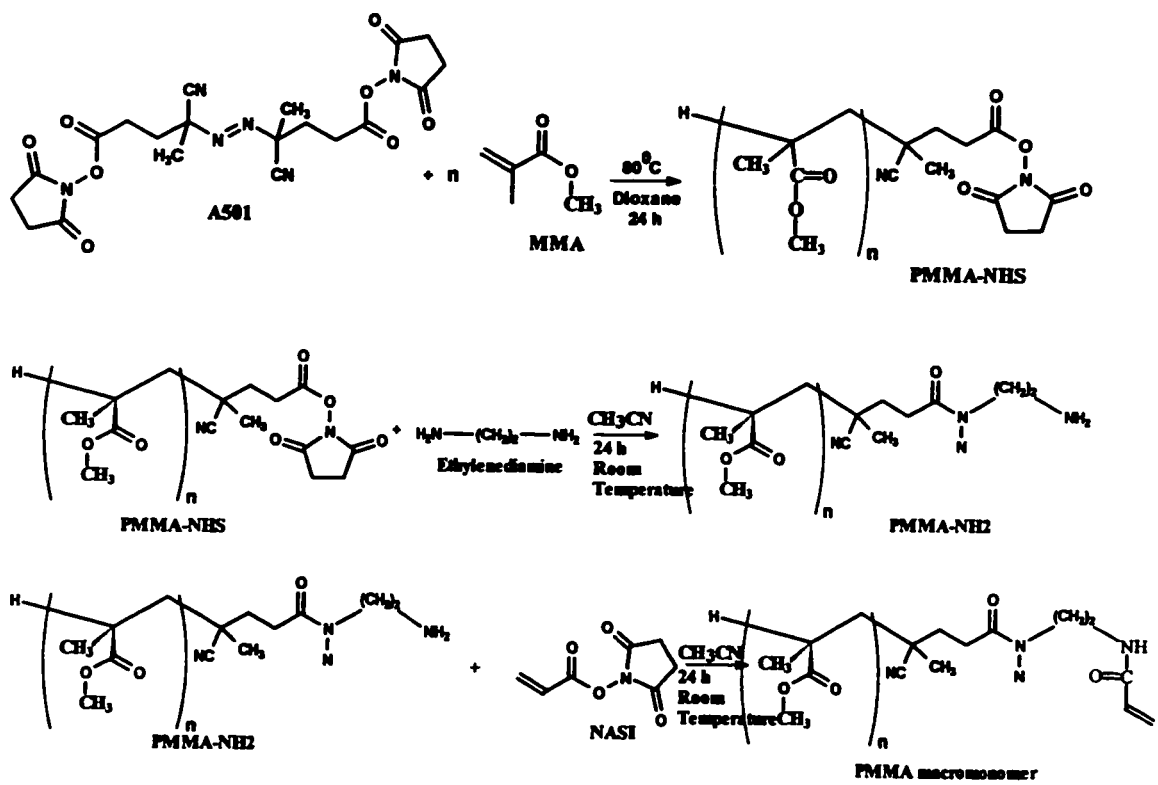


Figure 2. PMMA macromonomer synthesis using amide condensation reaction.

The step 3 of Figure 2 is similar to step 2. That is, amine group of PMMA-NH₂ reacts with the succinimide of NASI and forms an amide bond. Since, NASI has a double bond, MMA polymer was introduced with a double bond at the end, making it a monomer. For this project, PMMA-NH₂ (0.5 g, 0.007 mmol) and NASI (0.0017 g, 0.01 mmol) were added to 10 ml acetonitrile. It was assumed that PMMA-NHS had 0.1 mol % NH₂, so 20 fold excess NASI was added. The reaction mixture was stirred at room temperature for 24 hours, and then PMMA macromonomer was precipitated in MeOH and dried under vacuum.

Semitelechelic MMA Macromonomer Synthesis

Semitelechelic MMA macromonomer was synthesized by reacting amino-terminated MMA semitelomer with NASI or acryloylchloride (AcCl). Synthesis of monofunctional primary amino-terminated polymers using free radical polymerization and chain terminating agent is relatively straight forward (De Boos 1973), and therefore employed in this project. Moreover, aliphatic mercaptans have a high radical chain transfer constant and can be readily obtained in pure form. We chose AET as a chain terminating agent. It had a terminal -SH and -NH₂ group. Using VA086, we were able to synthesize amino-terminated semitelechelic MMA. AET concentration was varied to influence the MW of the semi telomer. Table 1 summarizes the amount of MMA, VA086, and AET that were used to synthesize the MMA semi telomers.

Table 1. Amount of MMA, AET, VA086, and DMF that were used to synthesize semitelechelic MMA.

VA086 (1 mol %)	AET	MMA	DMF
0.14 g, 0.5 mmol	0.45 g, 4 mmol (8 mol %)	5 g, 50 mmol	50 ml
0.14 g, 0.5 mmol	0.57 g, 5 mmol (10 mol %)	5 g, 50 mmol	50 ml
0.14 g, 0.5 mmol	0.79 g, 7 mmol (14 mol %)	5 g, 50 mmol	50 ml
0.23 g, 0.8 mmol	0.18 g, 1.6 mmol (2 mol %)	8 g, 80 mmol	80 ml
0.23 g, 0.8 mmol	0.55 g, 4.8 mmol (6 mol %)	8 g, 80 mmol	80 ml
0.23 g, 0.8 mmol	1.27 g, 11.2 mmol (14 mol %)	8 g, 80 mmol	80 ml

Step 1 of Figure 3 outlines amino-terminated MMA telomer synthesis. In all these reactions, the amount of the initiator VA086 was kept at 1 mol %. The reaction mixture was purged with N₂ for 5 minutes. Then the reaction vessel was sealed off, and the telomerization was carried out for 43 hours at 90 °C. High temperature and long reaction hour were employed because of long half-life of VA086 at high temperature (t_{1/2}: 10 hr at Temp: 87 °C). Semitelechelic MMA-NH₂ was added to MeOH for precipitation. The MeOH was 100 times more than the reaction volume. Since precipitation was not obtained, NaOH (40 M) was then added to facilitate precipitation. Finally, water, 100 times more than the reaction volume, was added to completely precipitate the semi telomer. The semi telomer was collected using gravity filtration and washed until the pH was neutral. Then, the precipitant was lyophilized.

Step 2 of Figure 3 outlines the nucleophilic reaction between semitelechelic MMA-NH₂ and NASI. Semitelechelic MMA-NH₂ (0.9 g, 0.22 mmol) that was terminated with 10 mol % AET and NASI (0.5 g, 3 mmol) were mixed in 15 ml CHCl₃. The solution was stirred for 24 hours at room temperature. Semitelechelic MMA macromonomer was precipitated in 50/50 DMF/ water and lyophilized.

Step 3 of Figure 3 outlines macromonomer synthesis using a different method. Step 3 involves nucleophilic reaction between semitelechelic MMA-NH₂ and acryloyl chloride. The amount of reactants is summarized in Table 2. The reaction mixture was stirred at 4 °C overnight and the macromonomer was collected using gravity filtration after precipitating in water. The precipitant was lyophilized.

Table 2. The amount of semitelechelic MMA-NH₂ and acryloyl chloride that were used to synthesize semitelechelic MMA macromonomer.

Semitelechelic MMA-NH₂	Acryloyl Chloride	DMA
0.4 g, 0.096 mmol (10 % AET)	78 µL, 0.96 mmol	10 ml
6 g, 0.6 mmol (2 % AET)	1.9 ml, 1.2 mmol	140 ml
5 g, 0.8 mmol (6 % AET)	4.9 ml, 60 mmol	50 ml
4.8 g, 1.6 mmol (14 % AET)	11.4 ml, 140 mmol	50 ml

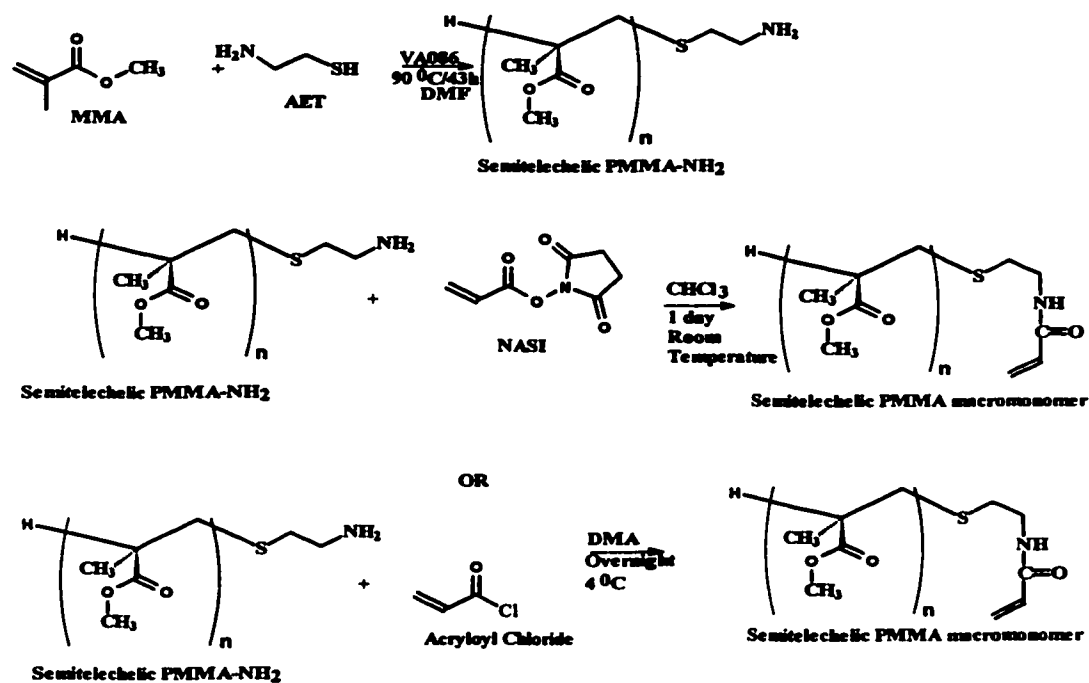
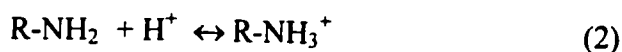


Figure 3. Semitelechelic PMMA macromonomer synthesis using telomerization and amide condensation reactions.

MW Determination of Semitelechelic MMA-NH₂

The number average MW of semitelechelic MMA-NH₂ was determined by titration of terminal amines using perchloric acid [Kaneko et al. 1995]. It was assumed that there was one amine group per semitelechelic MMA. Crystal violet (CV) was used as an indicator. At pH 2.6 or higher, CV gives blue-violet color to a solution. As the pH is gradually lowered to 0.0, the color of the CV solution changes from blue-violet to green and then to yellow.

For this project, polymer samples (0.1 g) were dissolved in 10 ml of acetic acid (CH₃COOH) and small amount of CV was added to the solution. Because of CV and high pH, the initial color of the polymer solution was blue-violet. The solution was then titrated with 0.1 M perchloric acid-acetic acid. Equations 1 and 2 outline the reactions during titration. Perchloric acid dissociates to H⁺ and ClO₄⁻ and the amine end group of polymer uptakes H⁺.



Where:

HClO₄: perchloric acid.

R: semitelechelic MMA

During titration, all the amine groups of the polymer were converted from R-NH₂ to R-NH₃⁺. Additional protons then reacted with CV. This changed the color of the polymer solution from blue-violet to green, and the titration was discontinued. The MW of semitelechelic MMA-NH₂ was calculated by dividing the mass of polymer sample with molar amount of added perchloric acid. Appendix A provides an example of MW calculation.

Synthesis of Random Polymer (RP) and Comb Polymer (CP)

The polymers were synthesized using a free radical polymerization process. Three types of anhydrous solvents were used: 1, 4-dioxane, t-butanol, and benzene. Polymerization was carried out in anhydrous solvents since A501 hydrolysis had to be

minimized. The glasswares were assembled as described in PMMA macromonomer synthesis. The monomers at the desired ratio were added to a round-bottom flask, followed by the addition of known amounts of A501. Solvent was added, and the solution was purged with N₂ while stirring with a magnetic stirrer. Finally, the round-bottom flask was sealed off. Polymerization was carried out for 24 hours at 80 °C.

Using the aforementioned method, two types of polymers were synthesized: random and comb-type polymers. RPs were prepared from the desired ratios of NiPAM, MMA, and AAc (see Table 3). CPs were synthesized from the desired ratios of NiPAM monomer and PMMA macromonomer (see Table 4) or semitelechelic PMMA macromonomer and AAc (see Tables 5, 6, 7, and 8). All polymers were precipitated in anhydrous diethyl ether.

Table 3. Amount of reactants that were used to synthesize RPs.

Polymer	Solvent	NiPAM	MMA	AAc	A501
RP1	30 ml dioxane	2.94 g, 26 mmol (98 mol %)	—	0.038 g, 0.53 mmol (2 mol %)	0.013 g, 0.027 mmol (0.1 mol %)
RP2	30 ml dioxane	2.79 g, 25 mmol (93 mol %)	0.13 g, 1.3 mmol (5 mol %)	0.038 g, 0.53 mmol (2 mol %)	0.013 g, 0.027 mmol (0.1 mol %)
RP3	30 ml dioxane	2.64 g, 23 mmol (88 mol %)	0.26 g, 2.6 mmol (10 mol %)	0.038 g, 0.53 mmol (2 mol %)	0.013 g, 0.027 mmol (0.1 mol %)
RP4	30 ml dioxane	2.49 g, 22 mmol (83 mol %)	0.40 g, 4.0 mmol (15 mol %)	0.038 g, 0.53 mmol (2 mol %)	0.013 g, 0.027 mmol (0.1 mol %)
RP5	30 ml benzene	2.94 g, 26 mmol (98 mol %)	—	0.038 g, 0.53 mmol (2 mol %)	0.013 g, 0.027 mmol (0.1 mol %)
RP6	30 ml benzene	2.49 g, 22 mmol (83 mol %)	0.40 g, 4.0 mmol (15 mol %)	0.038 g, 0.53 mmol (2 mol %)	0.013 g, 0.027 mmol (0.1 mol %)
RP7	15 ml dioxane	1.42 g, 12 mmol (95 mol %)	0.07 g, 0.7 mmol (5 mol %)	—	0.006 g, 0.013 mmol (0.1 mol %)

Table 4. Amount of reactants that were used to synthesize CPs with 72 kD MMA side chain.

Solvent	NiPAM	MMA	A501
10 ml t-butanol	0.95 g, 8.4 mmol (95 mol %)	0.044 g, 0.44 mmol (5 mol %)	0.0042 g, 0.009 mmol (0.1 mol %)
10 ml t-butanol	0.94 g, 8.3 mmol (94 mol %)	0.053 g, 0.53 mmol (6 mol %)	0.0042 g, 0.009 mmol (0.1 mol %)
10 ml t-butanol	0.93 g, 8.2 mmol (93 mol %)	0.062 g, 0.62 mmol (7 mol %)	0.0042 g, 0.009 mmol (0.1 mol %)
10 ml t-butanol	0.92 g, 8.1 mmol (92 mol %)	0.071 g, 0.71 mmol (8 mol %)	0.0042 g, 0.009 mmol (0.1 mol %)
10 ml t-butanol	0.80 g, 7.0 mmol (80 mol %)	0.18 g, 1.8 mmol (20 mol %)	0.0042 g, 0.009 mmol (0.1 mol %)

Table 5. Amount of reactants that were used to synthesize CPs with 10 kD MMA side chain.

Polymer	Solvent	NiPAM	MMA	AAc	A501
CP1	30 ml dioxane	2.79 g, 25 mmol (93 mol %)	0.13 g, 1.3 mmol (5 mol %)	0.038 g, 0.53 mmol (2 mol %)	0.013 g, 0.027 mmol (0.1 mol %)
CP2	30 ml benzene	2.79 g, 25 mmol (93 mol %)	0.13 g, 1.3 mmol (5 mol %)	0.038 g, 0.53 mmol (2 mol %)	0.013 g, 0.027 mmol (0.1 mol %)

Table 6. Amount of reactants that were used to synthesize CPs with 6 kD MMA side chain.

Polymer	Solvent	NiPAM	MMA	AAc	A501
CP3	30 ml dioxane	2.79 g, 25 mmol (93 mol %)	0.13 g, 1.3 mmol (5 mol %)	0.038 g, 0.53 mmol (2 mol %)	0.013 g, 0.027 mmol (0.1 mol %)
CP4	30 ml dioxane	2.64 g, 23 mmol (88 mol %)	0.26 g, 2.6 mmol (10 mol %)	0.038 g, 0.53 mmol (2 mol %)	0.013 g, 0.027 mmol (0.1 mol %)
CP5	10 ml dioxane	0.83 g, 7.3 mmol (83 mol %)	0.13 g, 1.3 mmol (15 mol %)	0.013 g, 0.18 mmol (2 mol %)	0.004 g, 8 μ mol (0.1 mol %)
CP6	30 ml benzene	2.79 g, 25 mmol (93 mol %)	0.13 g, 1.3 mmol (5 mol %)	0.038 g, 0.53 mmol (2 mol %)	0.013 g, 0.027 mmol (0.1 mol %)
CP7	30 ml benzene	2.64 g, 23 mmol (88 mol %)	0.26 g, 2.6 mmol (10 mol %)	0.038 g, 0.53 mmol (2 mol %)	0.013 g, 0.027 mmol (0.1 mol %)

Table 7. Amount of reactants that were used to synthesize CPs with 4 kD MMA side chain.

Polymer	Solvent	NiPAM	MMA	A501
CP14	15 ml dioxane	1.115 g, 9.9 mmol (93 mol %)	0.07 g, 0.7 mmol (7 mol %)	0.005 g, 0.01 mmol (0.1 mol %)

Table 8. Amount of reactants that were used to synthesize CPs with 3 kD MMA side chain.

Polymer	Solvent	NiPAM	MMA	AAc	A501
CP8	30 ml dioxane	2.79 g, 25 mmol (93 mol %)	0.13 g, 1.3 mmol (5 mol %)	0.038 g, 0.53 mmol (2 mol %)	0.013 g, 0.027 mmol (0.1 mol %)
CP9	30 ml dioxane	2.64 g, 23 mmol (88 mol %)	0.26 g, 2.6 mmol (10 mol %)	0.038 g, 0.53 mmol (2 mol %)	0.013 g, 0.027 mmol (0.1 mol %)
CP10	30 ml dioxane	2.49 g, 22 mmol (83 mol %)	0.40 g, 4.0 mmol (15 mol %)	0.038 g, 0.53 mmol (2 mol %)	0.013 g, 0.027 mmol (0.1 mol %)
CP11	30 ml benzene	2.79 g, 25 mmol (93 mol %)	0.13 g, 1.3 mmol (5 mol %)	0.038 g, 0.53 mmol (2 mol %)	0.013 g, 0.027 mmol (0.1 mol %)
CP12	30 ml benzene	2.64 g, 23 mmol (88 mol %)	0.26 g, 2.6 mmol (10 mol %)	0.038 g, 0.53 mmol (2 mol %)	0.013 g, 0.027 mmol (0.1 mol %)
CP13	30 ml benzene	2.49 g, 22 mmol (83 mol %)	0.40 g, 4.0 mmol (15 mol %)	0.038 g, 0.53 mmol (2 mol %)	0.013 g, 0.027 mmol (0.1 mol %)

NiPAM and MMA Contents of the Polymer

The composition of the synthesized polymers was determined using proton Nuclear Magnetic Resonance (NMR) spectroscopy. The polymers were dissolved in CDCl_3 , so the final concentration was 10 mg/ml. The chemical shifts for NiPAM and MMA were at 4.1 ppm and 3.6 ppm, respectively (see Figure 4). The peak areas were normalized for the number of hydrogens present in each peak.

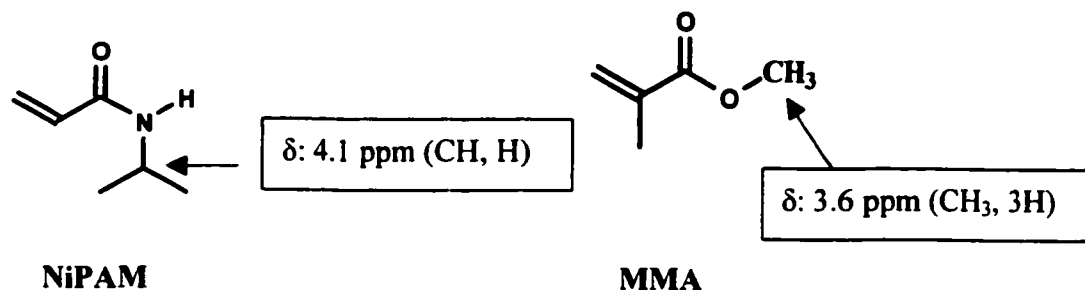


Figure 4. The chemical shifts for NiPAM and MMA.

Appendix B shows a sample NMR spectrum and a sample calculation that was used to determine NiPAM and MMA content of a particular polymer.

Acrylic Acid (AAc) Contents of the Polymer

AAc content was determined by acid/base titration. In this method, 50 mg of the polymer samples were dissolved in 5 mL of distilled, deionized water. These solutions were then titrated with 0.01M of NaOH using phenolphthalein as an indicator. NaOH reacted with AAc in one to one ratio. At the neutralization point, phenolphthalein changed from colorless to pink. Appendix C outlines a sample calculation that was used to determine AAc content of a particular polymer.

Succinimide Contents of the Polymer

Succinimide content was determined by modifying a spectrophotometric method that was described in [Miron and Wilchek 1982]. In this spectrophotometric assay, weak base, such as NH_4OH aminolyzes N-hydroxysuccinimide ester and releases ionized N-hydroxysuccinimide. The ionized N-hydroxysuccinimide gives an absorption peak at 260 nm, which allows quantitative measurement of NHS in polymers.

For this project, polymer samples were dissolved in CHCl_3 at 10 mg/mL. Then the polymer sample (1 mL) was reacted with excess (130 μL) 1.0 M NH_4OH (MeOH was used as the solvent) to release all NHS from the polymer. The change in absorbance at 260 nm was determined (Cary 50; Varian Inc.) and used as a measure of NHS concentration. The absorbance of polymers without NH_4OH was subtracted from

the absorbance of polymers with NH_4OH to account for the polymer background. A calibration curve for the spectroscopic assay was based on the aminolysis of A501. Briefly, A501 was dissolved in CHCl_3 at 1 mg/mL. A linear standard curve was obtained by diluting 1, 5, 10, 30, 70, 90, and 110 μL of 1 mg/mL A501 with MeOH, so the final volume was 1 mL. To these standard solution 130 μL of 1.0 M NH_4OH was added to release all the NHS, and the absorbance was measured at 260 nm. Appendix D shows the standard curve and outlines a sample calculation that was used to determine the NHS content of the polymer.

Weight-Average MW of the Polymer

The MW of RPs and CPs were determined by high-pressure liquid chromatography using a 7.8 x 300 mm StyragelTM HMW 6E GPC column (Waters Inc.). The polymer elution was detected by a combination of refractive index (Waters 410) and 90⁰ static light scattering detectors (PD2000; Precision Detectors, Andover, MA). Light scattering is a process in which light from a polarized laser beam is scattered in all directions upon interaction with a molecule or particle in a solution. The intensity of light and the angle of the scattered light depend on the MW or size of the molecule and the concentration of the solution. From this relationship, following formulae can be derived (from 1999 Precision Detector Inc. user manual):

$$I_{LS} = K_2 c \text{ MW } (dn/dc)^2 \quad (3)$$

Where:

I_{LS} = the light scattering signal intensity

K_2 = calibration constant

c = solution concentration in each chromatographic slice

dn/dc = the refractive index increment.

A refractive index measurement is used to determine the concentration of sample in each chromatographic slice, which is represented in the following formulae (from 1999 Precision Detector Inc. user manual):

$$c = I_{RI}/K_1(dn/dc) \quad (4)$$

Where:

I_{RI} = refractometer signal intensity

K_1 = calibration constant

In a typical run, a 20 μ L of polymer solution (10 mg/mL in THF) was injected onto the column by an autoinjector and the elution was performed with THF at 1 mL/min. The MW of the polymer was estimated using Precision MW Analysis software, which combines the aforementioned formula to produce the following formulae:

$$MW = K_2 \cdot I_{LS}/K_1 \cdot I_{RI} \cdot (dn/dc) \quad (5)$$

For a copolymer comprising monomers A and B or a terpolymer comprising units A, B, and C the refractive index increment is an additive function of the composition of the polymer expressed in terms of weight fraction w , thus (Huglin 1989):

$$dn/dc_{(AB \text{ polymer})} = w_A (dn/dc)_A + w_B (dn/dc)_B \quad (6)$$

$$dn/dc_{(ABC \text{ polymer})} = w_A (dn/dc)_A + w_B (dn/dc)_B + w_C (dn/dc)_C \quad (7)$$

In this case, the polymers were composed of NiPAM and MMA or NiPAM, MMA, and AAc. Since, refractive index increment of MMA and AAc had negligible effect on the MW calculation due to their small weight fraction, dn/dc of NiPAM polymer, which is 0.107 at 20 $^{\circ}$ C in THF [Zhou et al. 1995], was used to simplify the MW calculation. K_1 and K_2 were obtained by using polystyrene standards.

LCST by Spectroscopy

Polymers (5 mg/mL) were dissolved in 0.1 M phosphate buffer with (pH = 7.4) at 4 $^{\circ}$ C. 1 mL of polymer solution was added into a cuvette that was placed in a spectrophotometer (Ultraspect 2000; Pharmacia) equipped with a water-circulation cell. The water temperature was raised from 6 $^{\circ}$ C until phase inversion (in 1 $^{\circ}$ C

increments every 5 minutes) using a refrigerated/heated water circulator and the optical density (O. D.) was determined at 420 nm. Actual temperature of the samples was routinely measured with a digital thermometer by inserting into the samples. O. D. was plotted against temperature and the data was fitted to a sigmoidal curve and the LCST was taken as the middle of the inflection point. Appendix E shows a sample LCST plot of a particular polymer.

NASI Aminolysis Rate

During aminolysis, terminal amine of PMMA-NH₂ or semitelechelic MMA-NH₂ released the ionized NHS from NASI. The absorption peak of ionized NHS at 260 nm was monitored for 30 minutes, and then absorption (Abs.) versus time curve was fitted to a following first order equation using the SWIFT kinetic software:

$$A(t) = A_0 + (A_\infty - A_0) \cdot (1 - e^{-kt}) \quad (8)$$

where:

A(t) = absorbance over time

A₀ = initial absorbance

A_∞ = final absorbance

k = observed reaction rate

k_{obsd} was then calculated from this equation using SWIFT kinetic software. k_{obsd} is composed of following equation:

$$k_{obsd} = k_{hyd} + k_{am} [amine] \quad (9)$$

where:

k_{hyd.} = rate of NASI hydrolysis

k_{am.} = rate of NASI aminolysis

k_{obsd} was plotted as function amine (i.e. polymer) concentration, and the slope was used to calculate k_{am.} .

The polymer solutions were prepared in CH₃CN (Semitelechelic MMA-NH₂ was prepared in 50/50 = MeOH/CH₃CN). Typically, a range of polymer solutions (3 mg/ml – 20 mg/ml) was added to 0.15 mM of NASI and increase in Abs. at 260 nm as a function of time (30 minutes) was monitored.

Degelation of Polymer Gels

The purpose of degelation experiment was to study gel stability as the dissolution force became stronger. Dissolution force was increased by decreasing the temperature of the hydrogel. Polymers were dissolved in 0.1 M phosphate buffer (pH = 7.4) at 20 mg/ml with 5% DMF at 4 °C. Polymer solutions (2 mL) were then transferred to a 24 well cell culture plate. Hydrogels formed after incubating the solutions at 37 °C for 1 day. Gel resiliency was then determined by measuring the absorbance at 490 nm, using EL_x 800 Universal Microplate Reader (BioTek Instruments Inc.) as the temperature was lowered at 3 °C/day. Actual temperature of the solutions was determined by measuring the temperature of the phosphate buffer in one of the wells. The absorbance at 37 °C was taken as 100% and was used to normalize the rest of the absorbencies.

Bovine Serum Albumin (BSA) Conjugation to End-functionalized Polymer

End-functionalized polymer conjugation to protein was studied using BSA. RP 7 and CP14 were dissolved in anhydrous DMF at a concentration of 280 mg/ml. BSA solution was prepared at 1 mg/ml in 0.1 M phosphate buffer solution (PBS) (pH = 7.4). Protein and polymer solution were then added together to give final polymer concentrations of 18, 37, and 56 mg/ml and the final protein concentration of 0.4 mg/ml. An additional solution was prepared that had 56 mg/ml polymer and 0.4 mg/ml BSA. 10 µL 50 mM ethanolamine was added to the solution. All the mixtures were incubated at 4 °C for 24 hours. The reaction mixture was then diluted with electrophoresis buffer (62.5 mM Tris-HCl, 10% (V/V) glycerol, 2% (w/v) SDS, 0.05% (w/v) bromphenol blue) and loaded directly onto SDS-PAGE gel (4% acrylamide/N'N-bis-methylene-acrylamide concentration). The gel was stained with Coumassie R-250.

RESULTS

Overall Approach

The goal of this project was to synthesize end-functionalized CP with better gel stability than that of RP. CP and RP differ in their molecular architecture (shown in Figure 5). In RP, MMA is randomly distributed in NiPAM-AAc backbone. In CP, MMA chain branches out from NiPAM-AAc backbone. The objective of this project was to study the effect of the MW of NiPAM backbone and MMA chain on LCST and gel property. Therefore, high and low MW RPs and CPs (shown in Figure 5) were synthesized. The CPs had different lengths of MMA side chains (shown in Figure 5).

The CP synthesis was achieved in two phases. In Phase I, a methodology was developed for the synthesis of MMA macromonomer—a MMA polymer or MMA semitelomer with terminal double bond. MMA macromonomer is essential for CP synthesis. In first attempt, a MMA macromonomer with a MW of 72 kD was synthesized and used to synthesize CPs. However, the CPs were insoluble in PBS and, therefore, were unprocessable. Moreover, the CPs were difficult to purify because of the large MW of MMA macromonomer. During the second attempt, MMA macromonomers with lower MWs using telmerization technique were synthesized.

In Phase II, the effect of molecular architecture (CP vs. RP) and MW of MMA side chain and NiPAM backbone on physical properties of polymers was investigated. In this case, three types of CPs using the semitelehelic MMA macromonomer was synthesized. These CPs differed in their length of MMA branches. The MW of MMA branches were 3, 6, and 10 kD. Despite the low MW of MMA side chains, the CPs were insoluble. To improve solubility, 2 mol % AAc was added to all the CPs. The CPs were further divided according to their MW of NiPAM-AAc backbone. High MW polymers were synthesized from benzene, and low MW polymers were synthesized from dioxane. Besides CPs, high and low MW RPs were synthesized to investigate the effect of molecular architecture on LCST and gel stability. Certain RP and CP were reacted with BSA to qualitatively study end-functionalized polymer's capacity to conjugate to proteins.

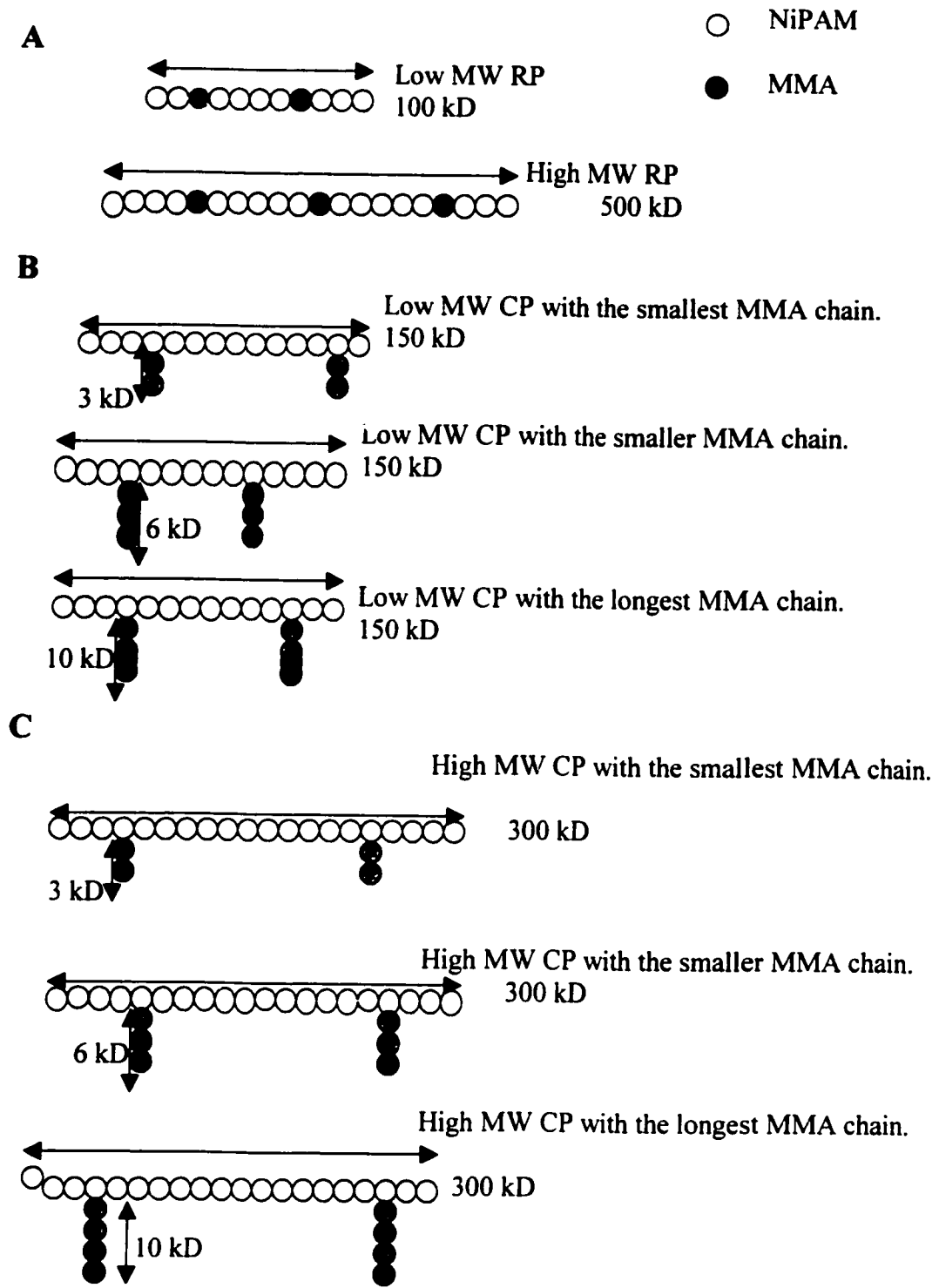


Figure 5. Molecular architecture of RP and CP. **A:** RP with low and high MWs. **B:** Low MW CP with MMA side chain between 3 and 10 kD. **C:** High MW RP with MMA side chain between 3 and 10 kD.

Phase I: Development of a Protocol for the Synthesis MMA Macromonomer

PMMA Macromonomer

PMMA macromonomer was synthesized as outlined in Materials and Methods. The MW of PMMA macromonomer was 72 kD, as determined by using size exclusion chromatography (SEC). I wanted to determine if the end-group, NASI, is capable of reacting with an amine reagent. Figure 6 shows that ethylenediamine or PMMA-NHS polymer has low absorbance at 260 nm. On the other hand, ethylenediamine reacts with the NHS of PMMA-NHS and releases the succinimide group (outlined in Step 2 of Figure 2). Since, succinimide group absorbs strongly at 260 nm, Figure 6 shows that when PMMA-NHS and diamine are mixed, there is an increase in absorbance at 260 nm. Figure 6, therefore, confirms that Step 1 of Figure 2 incorporates NHS at the end of MMA, and ethylenediamine reacts with NHS that converts the NHS terminated MMA to amino-terminated MMA (outlined in Step 2 of Figure 2). Excess NH_4OH was added to known amount of PMMA-NHS to release all the NHS group and the absorbance at 260 nm was measured. Then the calibration curve in appendix D was used to calculate number of moles of NHS/g of polymer. Then, by adding excess amount of ethylenediamine, PMMA-NHS was converted to PMMA- NH_2 (shown in Step 2 of Figure 2).

Next, we wanted to determine if the amine group of PMMA- NH_2 was reactive towards NASI. Figure 7 was obtained as outlined in Materials and Methods. Different concentration of PMMA- NH_2 was added to 0.15 mM NASI. k_{obs} was obtained by measuring the increase in absorbance at 260 nm for 30 minutes. Figure 7 was obtained by plotting k_{obs} as a function of PMMA- NH_2 concentration. k_{am} was obtained from the slope of figure 6, which was $0.4441 \text{ min}^{-1} \text{ mM}^{-1}$. A nonnegative and nonzero k_{am} showed that the amine of PMMA- NH_2 was reactive towards NASI as outlined in Step 3 of Figure 2. Overall, Figures 6 and 7 suggest that PMMA macromonomer can be synthesized using the scheme outlined in Figure 2. However, the 3 Hs (δ : 5.5-6.5 ppm) of PMMA macromonomer's terminal double bond cannot be detected using NMR because of the large MW (72 kD) of PMMA macromonomer; hence, formation of macromonomer cannot be independently confirmed.

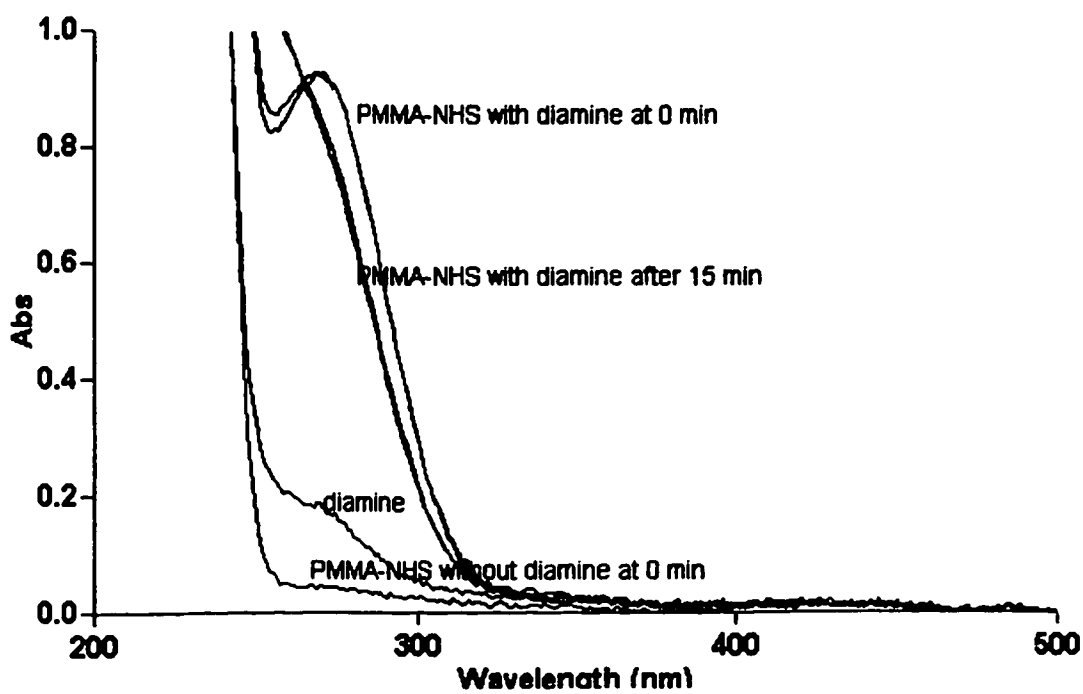


Figure 6. PMMA-NHS aminolysis using ethylenediamine.

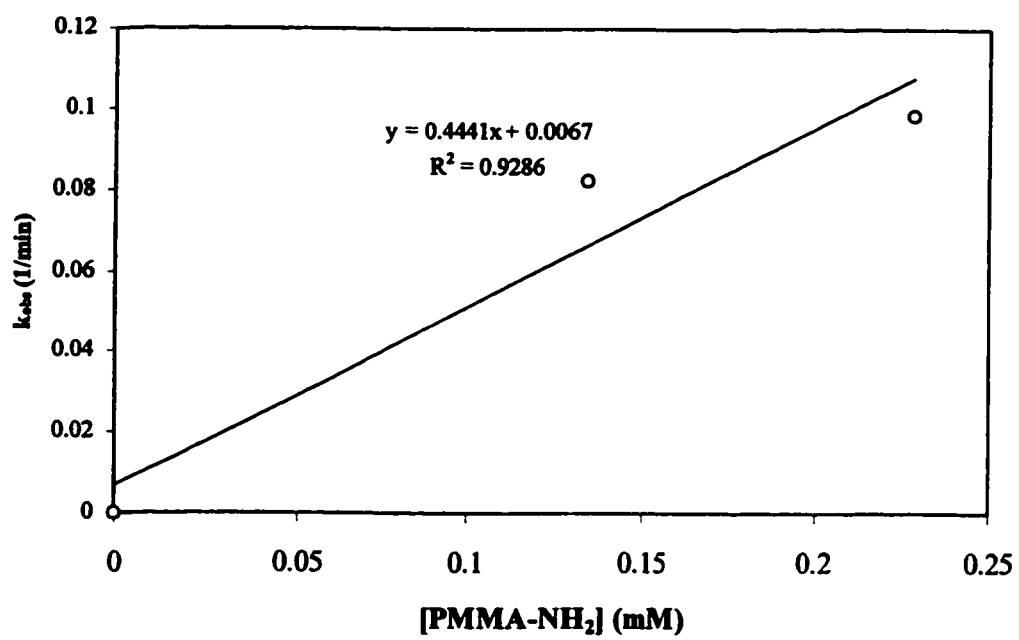


Figure 7. NASI aminolysis as a function of PMMA-NH₂.

Synthesis of Comb-Type Polymers

Table 9 summarizes the CPs that were synthesized using PMMA macromonomer. The MW of CPs were determined using SEC. t-butanol, like benzene, has low chain transfer constant. t-butanol was chosen to synthesize high MW CP, so the NiPAM backbone can control the polymer properties despite having 72 kD MMA branches.

Table 9. LCST and MWs of CP. NA means no analysis was done.

Solvent	% Feed Ratio (NiPAM: MMA)	% Observed Ratio (NiPAM: MMA)	$M_w \pm SD$ (kD) (triplicates)	LCST ($^{\circ}C$)
t-butanol	95:5	NA	900 ± 900	Insoluble
t-butanol	94:6	NA	NA	Insoluble
t-butanol	93:7	NA	NA	Insoluble
t-butanol	92:8	NA	580 ± 32	Insoluble
t-butanol	80:20	88:12	NA	Insoluble

One common observation with these polymers was the insolubility of polymers in PBS. During free radical reaction with these polymers, there are three theoretical possibilities for the final polymers: (a) NiPAM homo polymers, (b) NiPAM-MMA copolymers, and (c) MMA homo polymers. NiPAM homo polymer was expected to have an LCST between 30-32 $^{\circ}C$. In this case, the CPs were insoluble, which suggests that the 72 kD hydrophobic MMA macromonomers were incorporated in CP. MMA homo polymers did not form because NiPAM homo polymers would have formed too. As a result, we would observe phase separation at 30-32 $^{\circ}C$.

This first study indicated two following critical issues with this method of CP preparation: (i) Unreacted PMMA macromonomer cannot be separated from the CPs based on solubility because both PMMA macromonomer and CP precipitate in diethyl ether. (ii) High MW MMA branches are making the CP insoluble and, therefore, unprocessable. Since the large MW of PMMA macromonomer is at the root of our problem, we decided to synthesize smaller MW PMMA macromonomers.

Synthesis of Semitelechelic MMA Macromonomer

Low MW MMA can be synthesized using chain terminating agent AET: SH-CH₂-CH₂-NH₂ [De Boos 1973]. This telomerization process generates amino terminated semitelechelic MMA by incorporating the SH of AET at the end of the MMA semitelomer. Table 10 shows that considerably small MW semitelechelic MMA-NH₂ can be synthesized by varying the mol % of AET (Step 1 of Figure 3 outlines the reaction scheme). The number average MW of semitelechelic MMA-NH₂ was determined through titration.

Table 10. MW of semi-telechelic PMMA-NH₂. Standard Deviation: 0.4 kD.

Mol % AET	Solvent	M _n (kD) (duplicate)
8	DMF	5.8
10	DMF	4.0
14	DMF	3.1

From our first attempt of synthesizing MMA macromonomer, we learned that the NASI reacts with the terminal amine group of MMA and adds a double bond at the end of MMA. So we used NASI reaction with the terminal NH₂ group to synthesize semitelechelic MMA macromonomer. Step 2 of Figure 3 outlines the reaction scheme.

K_{obs} was obtained by reacting semitelechelic MMA-NH₂ with NASI. Figure 8 shows the K_{obs} as a function of semitelechelic MMA-NH₂ concentration. Figure 8 provides evidence that the semitelechelic MMA-NH₂ has functional amine groups, and the amine groups react with NASI (k_{am} > 0). Hence, semitelechelic MMA macromonomer should form when semitelechelic MMA-NH₂ is reacted in the presence of excess NASI. Moreover, since MW of semitelechelic PMMA-NH₂ is small, NMR spectrum of semitelechelic MMA macromonomer should have distinct vinyl peaks between 5.5 ppm and 6.5 ppm. A of Figure 9 shows that semitelechelic (10 mol % AET) MMA-NH₂ does not have vinyl peaks between 5.5 ppm and 6.5 ppm. B of Figure 9 is the NMR spectrum of semitelechelic MMA macromonomer that was synthesized by reacting semitelechelic (10 mol % AET, 4 kD) MMA-NH₂ with NASI.

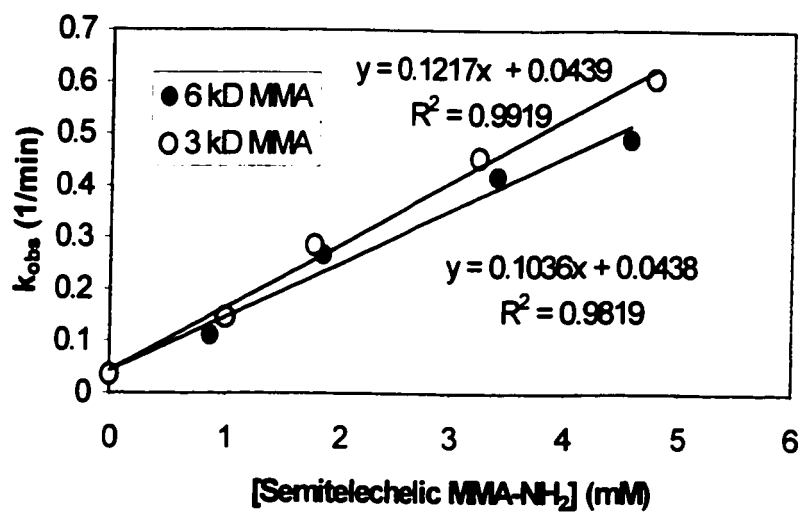
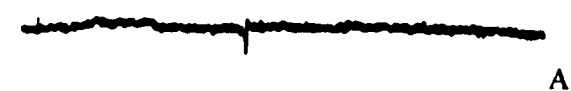
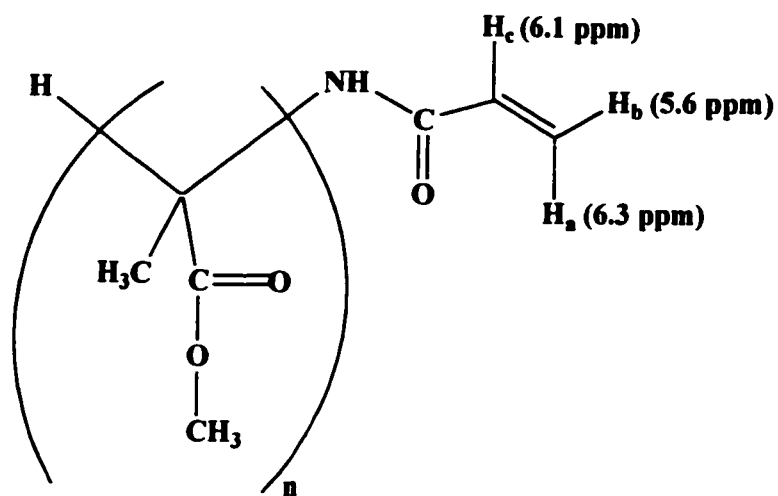


Figure 8. NASI aminolysis as a function of semitelechelic MMA-NH₂.



A



B



C

Figure 9. Appearance of Vinyl Peaks (between 5.5 and 6.5 ppm) in the NMR Spectrum of Semitelechelic MMA Macromonomer. A is Semitelechelic (10 mol % AET) MMA-NH₂, B is Semitelechelic (10 mol %) PMMA-NH₂ after reaction with NASI, and C is Semitelechelic (10 mol %) PMMA-NH₂ after reaction with acryloylchloride. The chemical structure depicts semitelechelic MMA macromonomer.

It shows that vinyl peaks are hardly detectable even after 1000X scans. This suggests that the reaction between PMMA-NH₂ and NASI is not very efficient.

Carbonyl group (C=O) of acryloylchloride (AcCl) is more nucleophilic than the carbonyl group of NASI since chloride is highly electrophilic. As a result, AcCl is more reactive towards amine than NASI, so we reacted semitelechelic PMMA-NH₂ (that was terminated with 10% AET) with AcCl (Step 3 of Figure 3). As a result, in contrast to B, C of Figure 8 shows distinct vinyl peaks. This independently confirms the formation of semitelechelic MMA macromonomer.

Phase II: Synthesis and Characterization of CP and RP

Synthesis of Semitelechelic MMA Macromonomer

In Phase II, the effect of the length or MW of MMA side chain on the CPs physical properties (e.g., LCST and gel stability) was investigated. Therefore, semitelechelic MMA-NH₂ with different MWs were synthesized. Table 11 shows that the MW of semitelechelic MMA-NH₂ can be varied by using different amount of AET. Figure 10 was obtained by plotting the MW of MMA semitelomers from Phase I and II as a function of mol % of AET. It shows that, as expected, the MW of MMA semitelomer decreases with the increase in mol % AET. This suggests that at higher mol % of AET, MMA semitelomers are terminated faster, so MW decreases with the increase in mol % AET. The number average MW of the semitelomer was determined using titration.

Table 11. MW of semi-telechelic PMMA-NH₂. Standard Deviation of average MW was less than 0.4 kD.

Mol % AET	Solvent	MW (kD) (duplicate)
2	DMF	10.4
6	DMF	6.0
14	DMF	3.0

As devised in Phase I, the semitelechelic MMA macromonomer was synthesized by reacting AcCl with the semitelechelic MMA-NH₂ (see the reaction scheme in Figure 2).

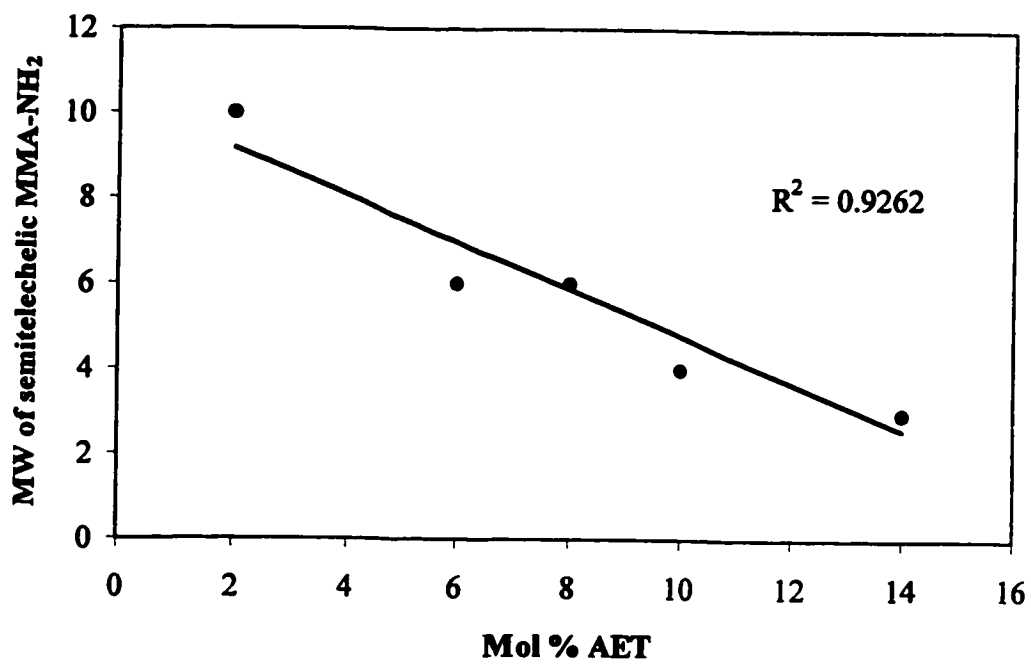


Figure 10. MW of semitelechelic MMA-NH₂ as a function of mol % AET.

Comb-Type Polymers (CPs)

CPs with 3 kD MMA side chains with MMA feed ratios 5, 10, and 15% were synthesized. Semitelechelic MMA macromonomer was soluble in diethyl ether, so it did not precipitate with CP. As a result, additional purification steps were not required. Uludag and coworkers found that the random NiPAM polymer with mol % MMA as high as 20.9 dissolved in water [2000]. It was found that the CPs with 3 kD MMA branches and 5 % MMA feed ratio (feed ratio is usually equivalent to final ratio) would not dissolve in PBS at 4 °C. To improve polymer solubility, we added a hydrophilic monomer AAc. AAc content of the polymer was kept low (2 mol %), so it did not interfere with the physical properties such as, LCST. 2 mol % AAc improved the polymer solubility, so their LCST was investigated.

Tables 12-14 summarize the physical properties of the CPs. The CPs are divided into three groups based on the length of MMA side chain: 10 kD (Table 12), 6 kD (Table 13), and 3 kD (Table 14). CPs with different length of MMA chain was synthesized, so the effect of MMA's MW on polymers' physical properties such as, LCST and gel stability could be investigated. The effect of MW of NiPAM polymer on the LCST and gel stability was also investigated. Therefore, each table is further divided into categories based on the solvent that was used during synthesis. In comparison with benzene, dioxane has higher chain transfer constant, so dioxane was chosen to synthesize low molecular weight comb-type polymer and benzene to synthesize high molecular weight comb-type polymer (see Figure 12). Figure 12 was generated by plotting the average MW of CP that were synthesized in dioxane and benzene. The error bar indicates standard deviation. The MWs are listed in the 6th column of Tables 12-14. Figure 11 was obtained by plotting LCST as a function of AAc in CPs. Figure 11 shows that AAc has negligible effect on CPs' LCST, even though it made the CPs more hydrophilic.

Table 12. Physical Properties of CP (MW of MMA Macromonomer: 10 kD). Where indicated, results are mean \pm SD.

Polymer	Solvent	% Feed Ratio (NiPAM:MMA:AAc)	Observed NiPAM/MMA (%)	Observed AAc (%) n = 2	MW (kD) n = 3	M_w/M_n n = 3	LCST ($^{\circ}$ C) n = 2	[Succinimide] (mmol/mg polymer)
CP1	D	93:5:2	93.2/5	1.8 \pm 0.0	130 \pm 0.0	1.9 \pm 0.1	30.5 \pm 0.7	1.7 $\times 10^{-3}$
CP2	B	93:5:2	88.5/9.7	1.8 \pm 0.1	296 \pm 31	2.1 \pm 0.1	29.2 \pm 0.4	4.2 $\times 10^{-3}$

Table 13. Physical Properties of CP (MW of MMA Macromonomer: 6 kD). Where indicated, results are mean \pm SD.

Polymer	Solvent	% Feed Ratio (NiPAM:MMA:AAc)	Observed NiPAM/MMA (%)	Observed AAc (%) n = 2	MW (kD) n = 3	M_w/M_n n = 3	LCST ($^{\circ}$ C) n = 2	[Succinimide] (mmol/mg polymer)
CP3	D	93:5:2	93/5	2.0 \pm 0.1	120 \pm 17	2.2 \pm 0.3	30.5 \pm 0.7	2.4 $\times 10^{-3}$
CP4	D	88:10:2	88.5/9.2	2.3 \pm 0.1	95 \pm 4	2.0 \pm 0.4	31.7 \pm 0.7	2.4 $\times 10^{-3}$
CP5	D	83:15:2	86.1/11.5	2.4 \pm 0.1	100 \pm 0	1.9 \pm 0.0	29.5 \pm 1.1	2.1 $\times 10^{-3}$
CP6	B	93:5:2	91.4/6.7	1.9 \pm 0.1	266 \pm 32	2.0 \pm 0.1	30.2 \pm 0.6	3.3 $\times 10^{-3}$
CP7	B	88:10:2	90.5/6.3	3.2 \pm 0.0	486 \pm 65	2.8 \pm 0.3	32.1 \pm 0.7	2.1 $\times 10^{-3}$

Table 14. Physical Properties of CP (MW of MMA Macromonomer: 3 kD). * n = 1. Where indicated, results are mean \pm standard deviation. n is the number of samples that were used to determine a certain property.

Polymer	Solvent	% Feed Ratio (NiPAM: MMA: AAc)	Observed NiPAM/MMA (%)	AAc in Polymer(%) n = 2	MW (kD) n = 3	M_w/M_n n = 3	LCST ($^{\circ}$ C) n = 2	[Succinimide] (mmol/mg polymer)
CP8	D	93:5:2	93.8/3.2	3.0 \pm 0.4	233 \pm 68	3.1 \pm 0.6	30.5 \pm 0.7	1.9 $\times 10^{-3}$
CP9	D	88:10:2	91.3/7	1.8 \pm 0.0	146 \pm 12	2.6 \pm 0.2	30.5 \pm 0.7	1.8 $\times 10^{-3}$
CP10	D	83:15:2	88/9.7	2.2 \pm 0.1	92 \pm 2	2.4 \pm 0.2	32.0 \pm 0.7	2.2 $\times 10^{-3}$
CP11	B	93:5:2	89.3/8.6	2.0 \pm 0.0	620 \pm 193	2.5 \pm 0.5	29.5 \pm 0.7	2.8 $\times 10^{-3}$
CP12	B	88:10:2	86.7/11.2	2.0 \pm 0.0	373 \pm 87	2.1 \pm 0.3	28.5 \pm 0.7	5.5 $\times 10^{-3}$
CP13	B	83:15:2	85.8/11.6	2.5 \pm 0.1	956 \pm 169	2.1 \pm 0.1	33.5*	5.3 $\times 10^{-3}$

First column of Tables 12-14 is the identification of the individual polymer. Second column is the solvent that was used during polymerization. Mol % of NiPAM and MMA in CP was determined using NMR spectroscopy. NiPAM and MMA content of CPs are listed in the fourth column. Figure 13 was obtained by plotting the MMA composition of CP as a function % MMA in feed. It shows that the MMA content of CP plateaued as MMA feed ratio was increased. This suggests that at a high feed ratio (10 or 15 mol %), the MMA macromonomer is not readily incorporated in the CP. Fifth column lists the mol % AAc in CP. They were determined using titration. As expected, AAc composition of CP is similar to the AAc feed ratio during polymerization. Seventh column lists the polydispersity of the MW of CP. They were estimated using Precision MW Analysis software. Ideal polydispersity for free radical polymerization is 2. The polydispersities of CPs were between 2 and 3, which means the breadth of the MW distribution is not too wide. This suggests that the incorporation of semitelechelic MMA macromonomer does not interfere with the MW of polymer chain. Eighth column lists the LCSTs of the CPs. Figure 14 was obtained by plotting LCST as a function of MMA content of the CP. It shows that the LCSTs of CPs are independent of the hydrophobic MMA content of the polymer. The final column lists the succinimide contents of the polymers. Figure 15 was obtained by plotting the succinimide concentration as a function of MW. The figure shows that there is no correlation between the succinimide content and the MW of the polymer. This is unexpected because A501 initiates polymerization. As a result, NASI content (per g polymer basis) of the polymer suppose to increase, as MW gets smaller. The absence of correlation is due to high experimental variability such as, choice of solvent, MMA amount, temperature, etc. Solvent is responsible for terminating the polymerization. Hence, as shown in Figure 12, MW of CPs depends on the type of solvent that is used during polymer synthesis. Since, succinimide is present for all the CPs, we should be able to conjugate proteins to the polymers.

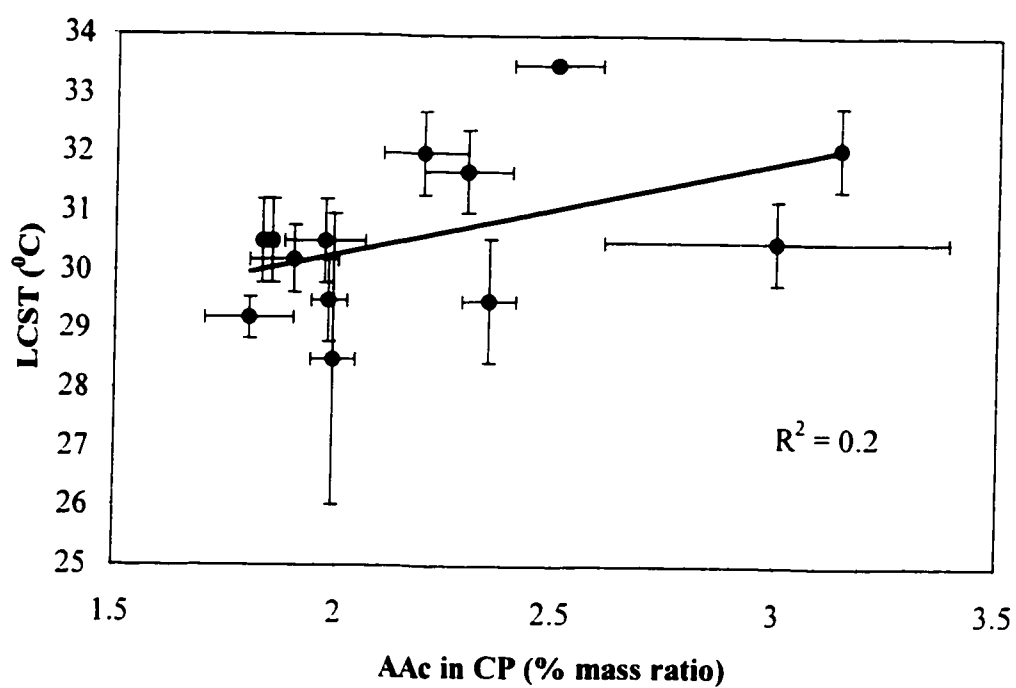


Figure 11. LCST of CP as a function of AAc in CP. The results are shown as mean \pm standard deviation. % mass ratios of AAc in CPs and the LCSTs of CPs were determined in duplicate.

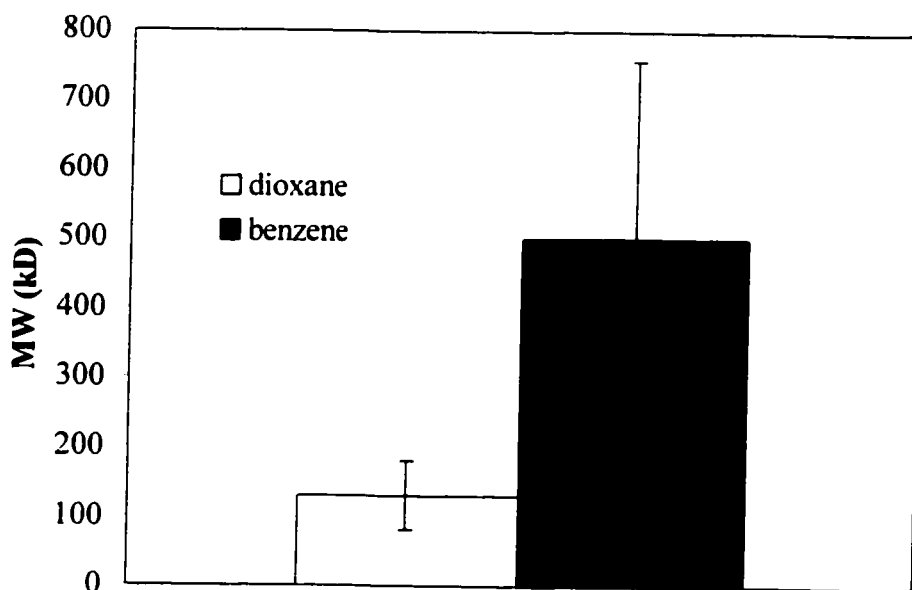


Figure 12. Low and high MW CPs synthesized in dioxane and benzene, respectively. The results are shown as mean \pm standard deviation of $n = 7$ for MWs of CPs synthesized in dioxane and $n = 6$ for MWs of CPs synthesized in benzene. The MW of each CP was determined in triplicate. The difference between the means is statistically significant (one sided p-value: 0.002).

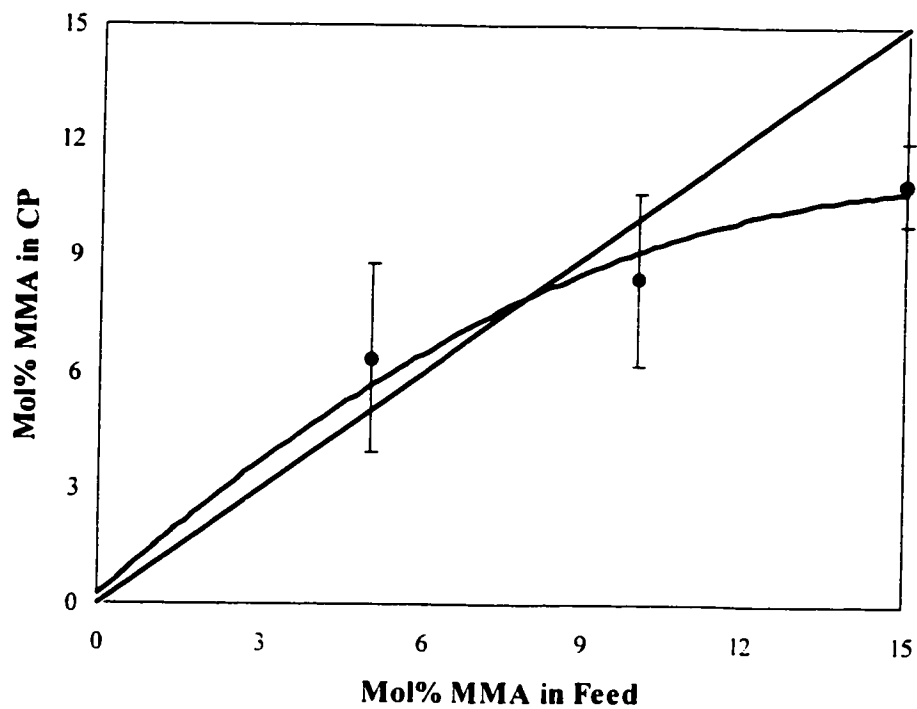


Figure 13. MMA composition of the synthesized CP as a function of MMA macromonomer in feed. The straight line in the graph represents 1:1 ratio of MMA in feed and observed MMA composition. The curved line represents the relationship between mol% MMA in feed and mol% MMA in CP. The results are shown as mean \pm standard deviation where $n = 2$, which is the number of CPs that were synthesized with the same mol% MMA macromonomer in feed.

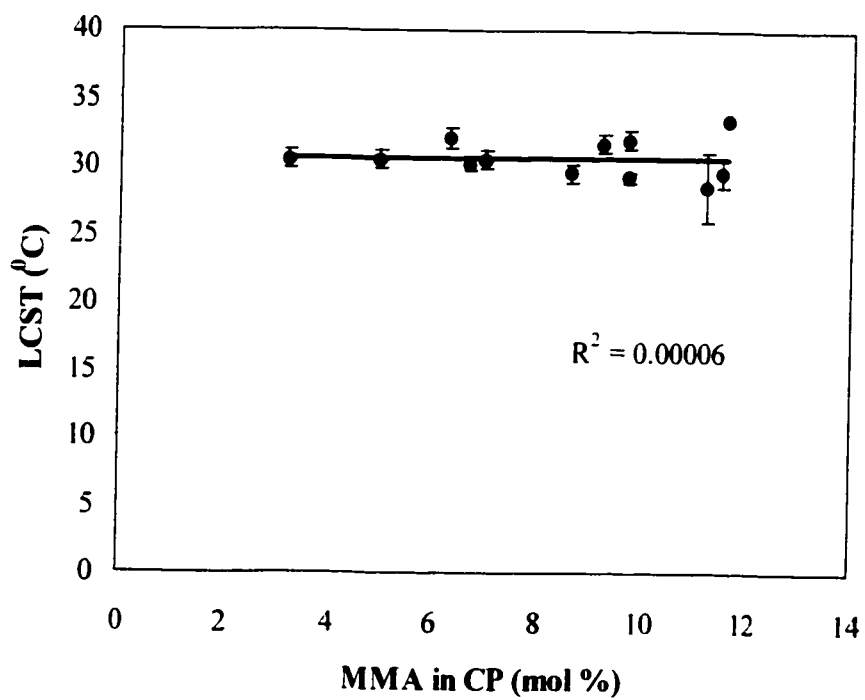


Figure 14. LCST of CP as a function of MMA in CP. The results are shown as mean \pm standard deviation. The LCSTs were determined in duplicate.

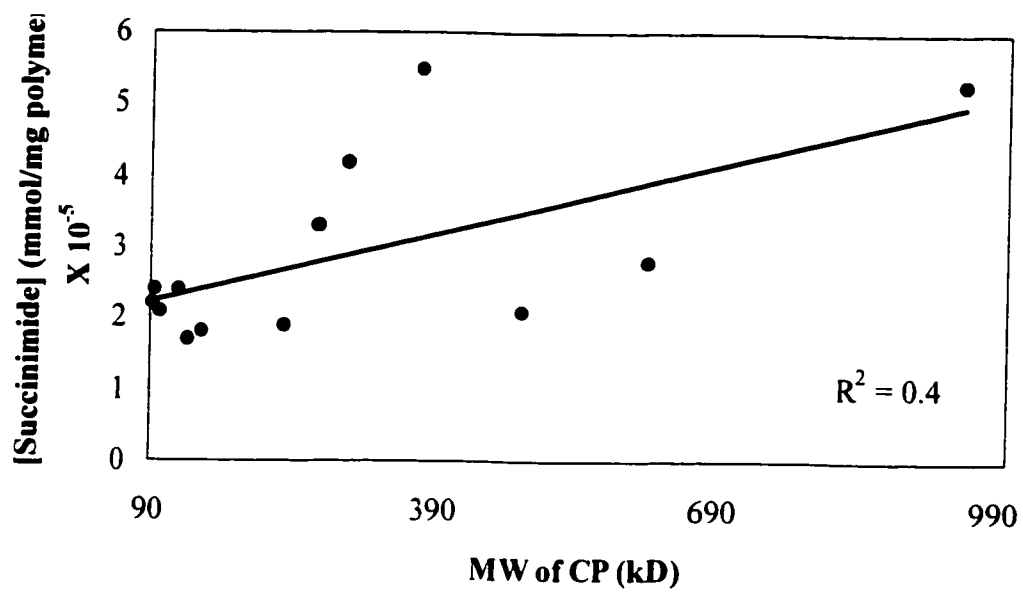


Figure 15. Succinimide concentration as a function of MW of CP.

Random Polymers (RPs)

RPs have different molecular architecture than CP. The hydrophobic units are randomly dispersed throughout the polymer chain. Table 15 summarizes the physical properties of the RPs that were synthesized for this project. Note that RP6 had two peaks on SEC spectrum. First peak was generated by 25 % of the polymer and second peak was generated by 75% of the polymer. The percentages were determined using the area under the peaks. MWs for individual peaks are shown. Seventh column lists the polydispersity of RPs. This shows that the MW distribution of RPs are as expected for polymers that are synthesized using the free radical polymerization technique. Eighth column lists the LCST of RPs. The final column lists the succinimide content of the RP.

Since the physical properties of the RP would be compared to that of CP, similar reaction conditions and monomers were employed to synthesize RP. Only difference in reaction condition between RP and CP was that MMA monomer, not semitelechelic MMA macromonomer, was used. Figure 18 was obtained by plotting the MMA content of RP as a function of MMA in feed. It shows that MMA monomer is incorporated in the polymer at a ratio proportional to the feed ratio. In contrast to CP, MMA content of RP does not decrease at high MMA feed ratio (10-15%).

Similar to CP, 2 mol % hydrophilic monomer AAc was added to RP. Figure 16 was obtained by plotting the AAc content of RP as a function of their LCST. Given the limited sample size and narrow range of AAc, Figure 16 shows that there is no correlation between RPs' LCST and AAc content. The MW of RP was also varied using benzene and dioxane. Figure 17 was obtained by plotting the average MW of RP that were synthesized in benzene and dioxane. Like in the case of CP, benzene generated high MW RP and dioxane generated low MW RP. Figure 19 was obtained by plotting the LCST of RP as a function of MMA content of the RP. It shows that the LCST of the RP decreased slightly (~ 4 °C by 15% MMA) with the increase in hydrophobic MMA content. Figure 20 shows that the succinimide concentration of RP is independent of the MW of the RP. In other words, solvent was the major terminating agent of RP.

Table 15. Physical Properties of RP. * Peaks on SEC spectrum. Where indicated, results are mean \pm standard deviation. n is the number of samples that were used to determine a particular property.

Polymer	Solvent	% Feed Ratio (NiPAM: MMA:AAC)	Observed NiPAM/MMA (%)	Observed AAC (%) n = 2	MW (kD) n = 3	M _w /M _n n = 3	LCST (°C) n = 2	[Succinimide] (mmol/mg polymer) X 10 ⁻⁵
RP1	D	98:0:2	98.2/0	1.8 \pm 0.0	356 \pm 146	3.2 \pm 0.3	29.0 \pm 0.0	6.0
RP2	D	93:5:2	89.3/8.9	1.8 \pm 0.1	143 \pm 6	1.6 \pm 0.1	28.0 \pm 0.0	4.7
RP3	D	88:10:2	88.3/9.9	1.8 \pm 0.1	110 \pm 0	1.8 \pm 0.2	28.0 \pm 0.0	6.8
RP4	D	83:15:2	82.5/15.7	1.8 \pm 0.1	110 \pm 0	1.7 \pm 0.1	25.0 \pm 0.0	5.5
RP5	B	98:0:2	98/0	2.0 \pm 0.01	160 \pm 44	1.3 \pm 0.2	29.2 \pm 0.4	6.2
RP6	B	83:15:2	82.8/15.2	2.0 \pm 0.2	6966 \pm 208 (25%)* 506 \pm 40 (75%)*	1.2 \pm 0.2 (25%)* 1.5 \pm 0.1 (75%)*	27.0 \pm 0.0	5.7

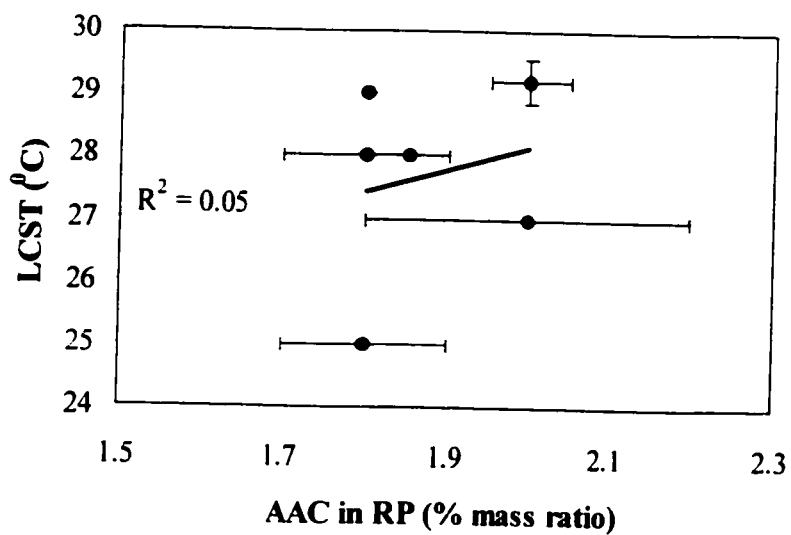


Figure 16. LCST of RP as a function of AAC in RP. The results are shown as mean \pm standard deviation. % mass ratios of AAC in RPs and the LCSTs of RPs were determined in duplicate.

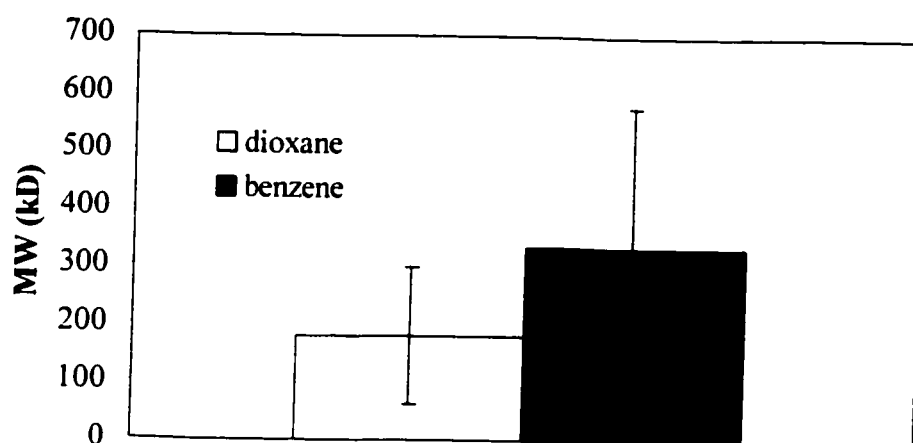


Figure 17. Low and high MW RPs synthesized in dioxane and benzene, respectively. The results are shown as mean \pm standard deviation of $n = 4$ for MWs of RPs synthesized in dioxane and $n = 2$ for MWs of RPs synthesized in benzene. The MW of each RP was determined in triplicate. The difference between the means is insignificant (one sided p-value: 0.2).

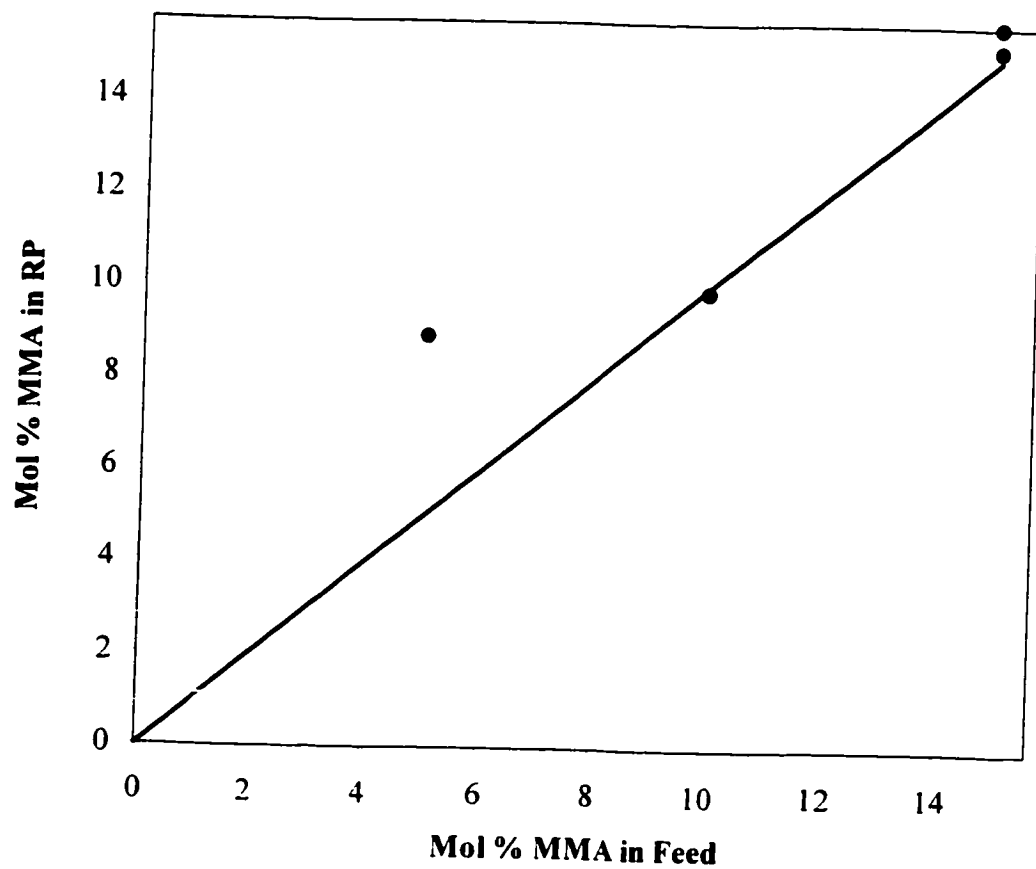


Figure 18. MMA composition of the synthesized RP as a function of MMA in feed. The straight line in the graph represents 1:1 ratio of MMA in feed and observed MMA composition.

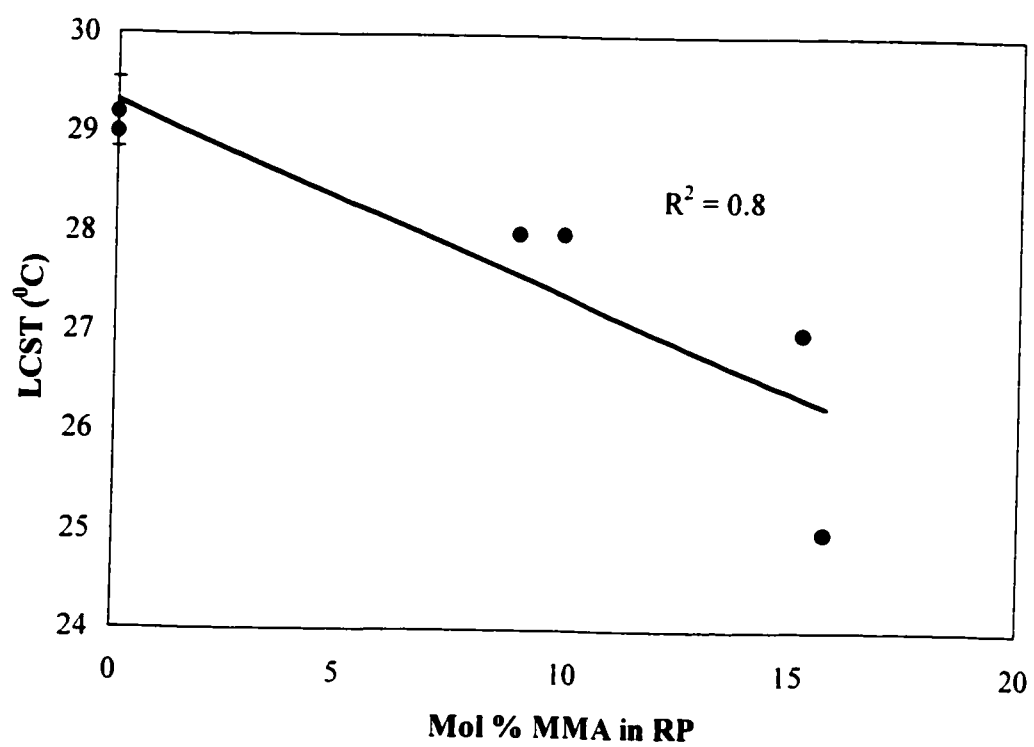


Figure 19. LCST of RP as a function of MMA in RP.

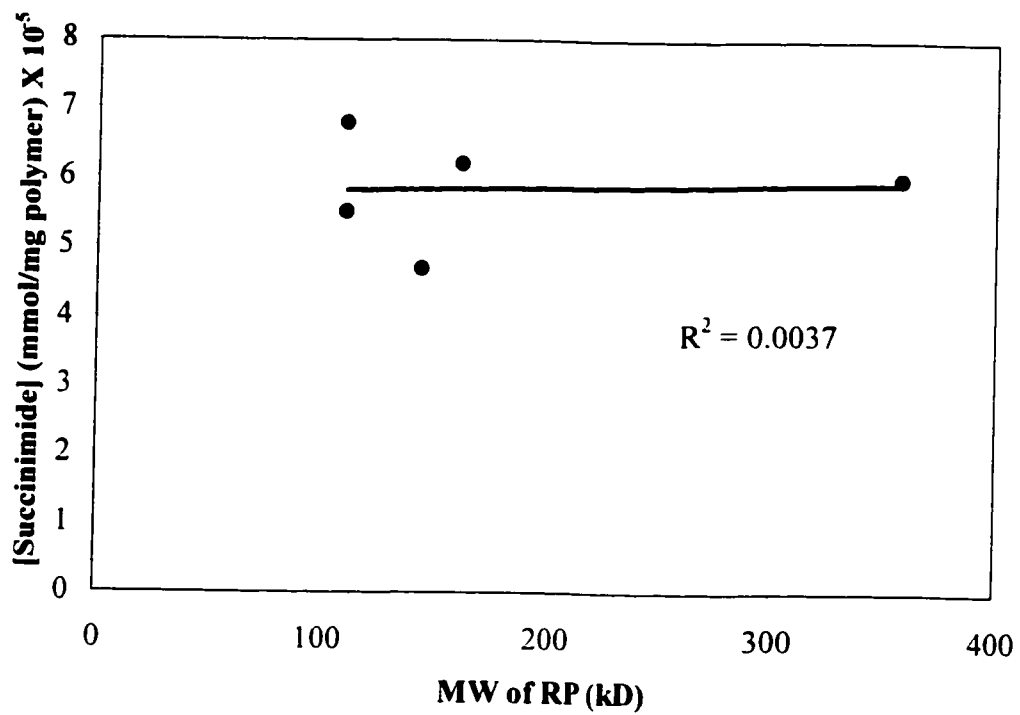


Figure 20. Succinimide concentration as a function of MW of RP.

Degelation of Hydrogels

From the results above, it is clear that all of the polymers, CP or RP, are capable of displaying an LCST below the physiological temperature. This is important but not the only requirement for the polymers to form stable gels *in vivo*. It is essential that the polymeric micelles display sufficient self-association for gelation. This phenomenon was studied using a hydrogel dissolution study. This approach determines gel stability as the driving force for dissolution becomes increasingly stronger (i.e., temperature goes down). For this project, hydrogels at 20 mg/ml were prepared at 37 °C. Their absorbance was measured at 490 nm while their temperature was decreased at 3 °C/day. The absorbance at 37 °C was designated as 100% and used to normalize the rest of the absorbencies. Figures 21-28 was obtained by plotting % absorbance of a hydrogel as a function of temperature.

T_{50} , the temperature at which the absorbance of the hydrogel decreases 50%, was calculated from these degelation curves to compare the hydrogel stability of the polymer. Table 16 lists the T_{50} and LCST of CP. Appendix F lists the raw data of CP1. The data was used to generate the degelation curve for CP1. It also shows the calculation that was used to determine % absorbance and the method that was used to determine T_{50} .

Figures 21-23 show the degelation curve of high and low MW CPs. The CPs of Figures 21-23 had different lengths of MMA side chains: 10, 6, and 3 kD. From these figures, following observation can be made about the CP hydrogels: hydrogel stability depends on the MW of the polymer. Figures 21-23 show that high MW CPs are more stable than the low MW CP. T_{50} is a good measurement for gel stability. Figure 30 shows that T_{50} decreases, i.e., gel stability improves, with the increase in MW of CP.

Figure 24 shows the degelation of high MW CPs with three different lengths of MMA side chain. Similarly, Figure 25 shows the degelation of low MW CPs with three different lengths of MMA side chain. From these figures, following observation can be made about the CP hydrogels: when MWs of CPs are similar length of MMA chain does not affect gel stability. Hence, all these hydrogels have similar T_{50} .

Figures 26 and 27 show degelation of high and low MW CPs that had different amount of 3 kD MMA side chain. These figures show that given the limited sample size and narrow range of MMA content, MMA of CP does not affect the hydrogel stability for both low MW and high MW CP.

Figure 28 shows the degelation curve of high MW RPs. Low MW RPs from dioxane did not gel, and therefore they were not shown. Table 17 lists the T_{50} and LCST of high MW RP hydrogel. Following observations can be made for the RP hydrogels: (a) For this project, MW of RP is important for hydrogel formation. High MW RP from benzene formed gel but low MW RP from dioxane did not. (b) Increase in MMA content lowers the LCST of RP but does not improve gel stability as can be seen in Figure 28. (c) T_{50} of high MW RP hydrogel is directly related to the RP's LCST (see Table 17). In contrast, the T_{50} of CP is independent of its LCST (see Table 16). Figure 29 illustrates this point.

Table 16. T_{50} of CP hydrogel.

Polymer	T_{50} ($^{\circ}$ C)	LCST ($^{\circ}$ C)
CP1	32.5	30.5
CP2	27.2	29.2
CP3	32.5	30.5
CP6	27	30.2
CP8	32.7	30.5
CP11	25.5	29.5

Table 17. T_{50} of high MW RP hydrogel

Polymer	T_{50} ($^{\circ}$ C)	LCST ($^{\circ}$ C)
RP5	29	29.2
RP6	27.5	27

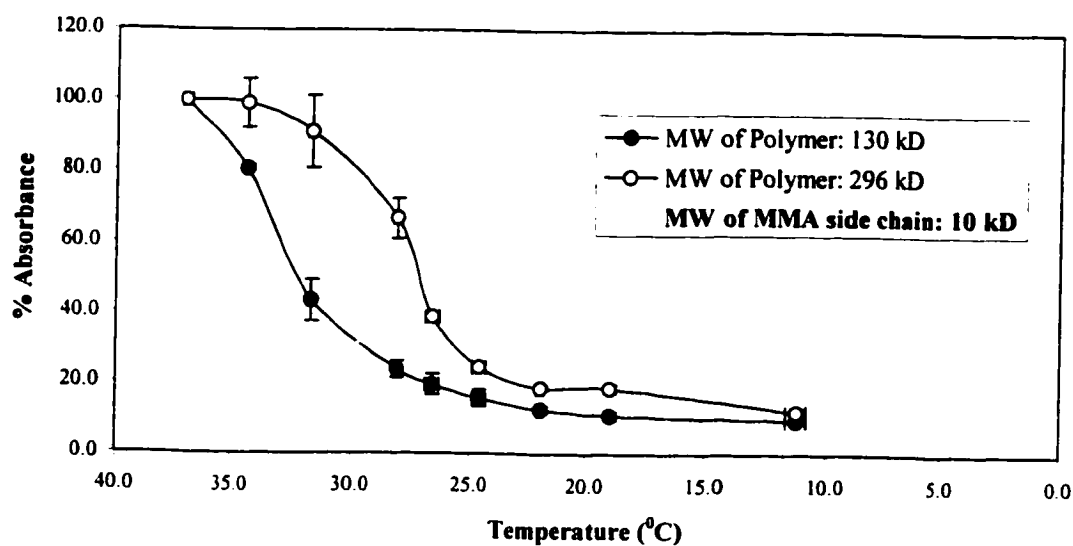


Figure 21. Degelation of high and low MW CP (CP2 and CP1, respectively). % of MMA: 5 (low MW), 9.7 (high MW). Where indicated, the results are mean \pm standard deviation of two samples. As the temperature was lowered, the % absorbance was reduced, until polymer was totally dissolved. At this point, % absorbance was 20%. The higher MW polymer exhibited a higher resiliency to dissolution, as evident by the need for a lower temperature to initiate dissolution.

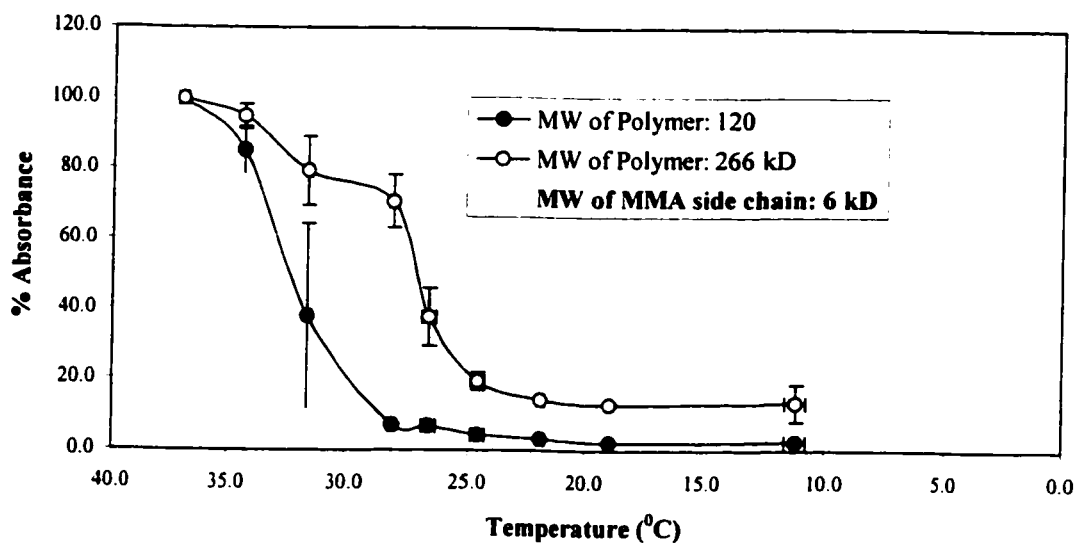


Figure 22. Degelation of CP with high and low MW (CP6 and CP3, respectively) (% of MMA: 5 (low MW); 6.7 (high MW). Where indicated, the results are mean \pm standard deviation of two samples. As the temperature was lowered, the % absorbance was reduced, until polymer was totally dissolved. At this point, % absorbance was 20% (for high MW polymer) and 5% (for low MW polymer). The higher MW polymer exhibited a higher resiliency to dissolution, as evident by the need for a lower temperature to initiate dissolution.

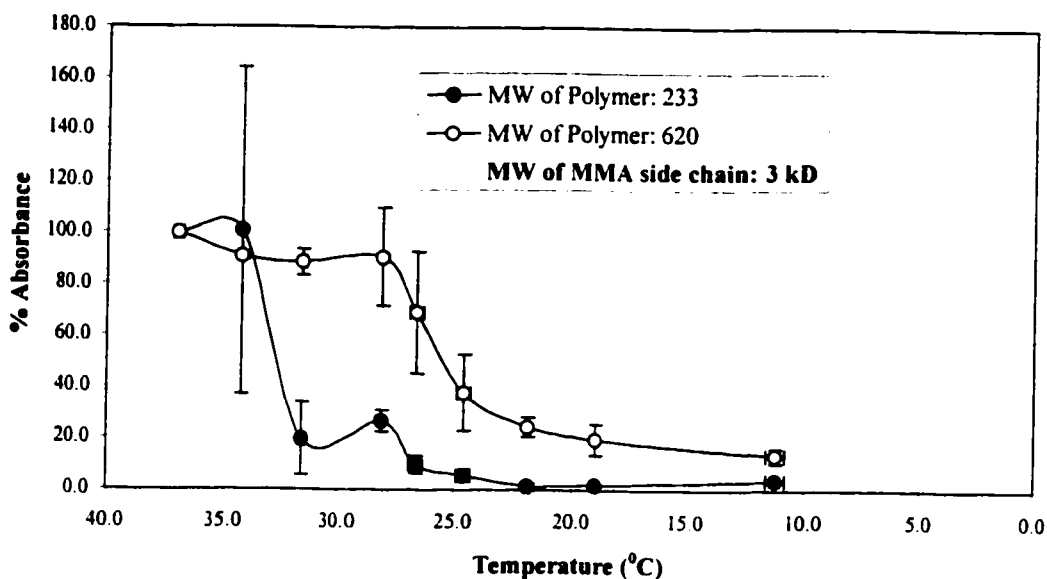


Figure 23. Degelation of CP with high and low MW (CP11 and CP8, respectively). % of MMA: 3.2 (low MW); 8.6 (high MW). Where indicated, the results are mean \pm standard deviation of two samples. As the temperature was lowered, the % absorbance was reduced, until polymer was totally dissolved. At this point, % absorbance was 15% (for high MW polymer) and 5% (for low MW polymer). The higher MW polymer exhibited a higher resiliency to dissolution, as evident by the need for a lower temperature to initiate dissolution.

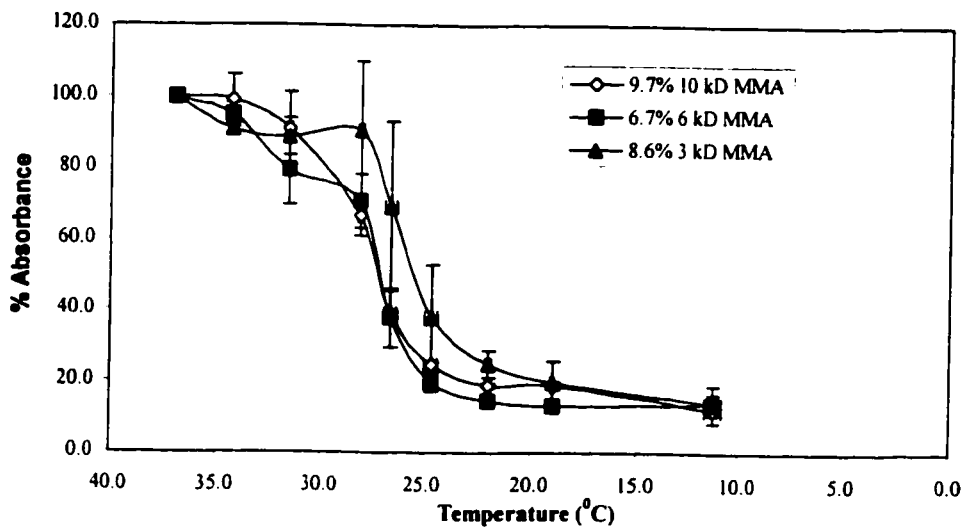


Figure 24. Degelation of high MW CP with different length of MMA side chain (CP2, CP6, and CP11, respectively). Where indicated, the results are mean \pm standard deviation of two samples. As the temperature was lowered, the % absorbance was reduced, until polymer was totally dissolved. At this point, % absorbance was 15%. The higher MW polymer with different length of MMA branches exhibited similar resiliency to dissolution, as evident by the need for a similar temperature to initiate dissolution.

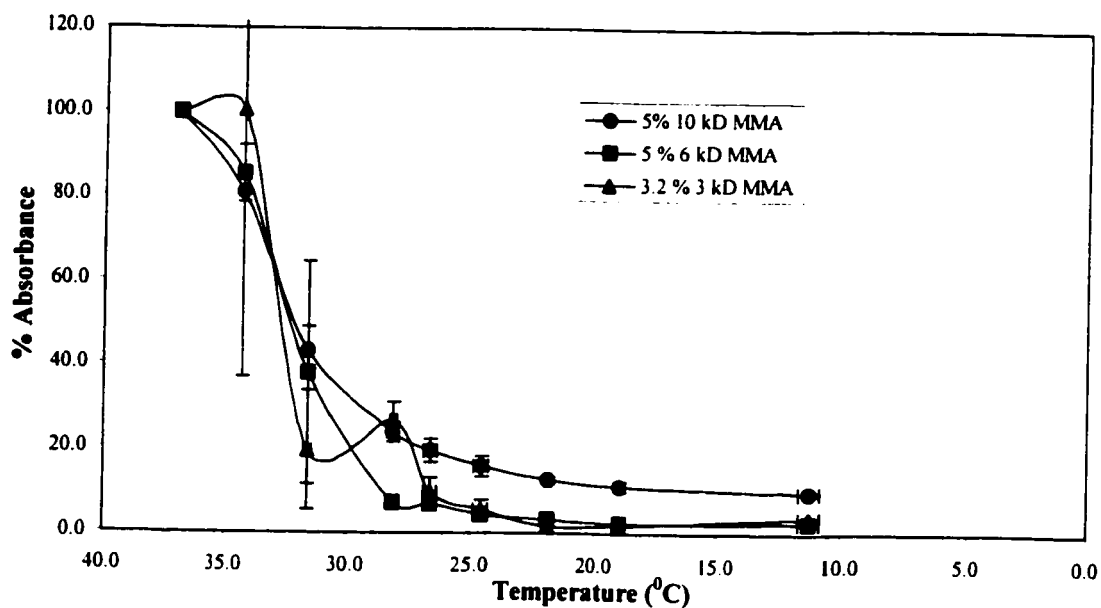


Figure 25. Degelation of low MW CP with different length of MMA side chain (CP1, CP3, and CP8, respectively). Where indicated, the results are mean \pm standard deviation of two samples. As the temperature was lowered, the % absorbance was reduced, until polymer was totally dissolved. At this point, % absorbance was between 15% and 5%. The low MW polymer with 10 kD MMA chains showed higher resiliency to dissolution than the other polymers even though initially they all exhibited similar resiliency to dissolution.

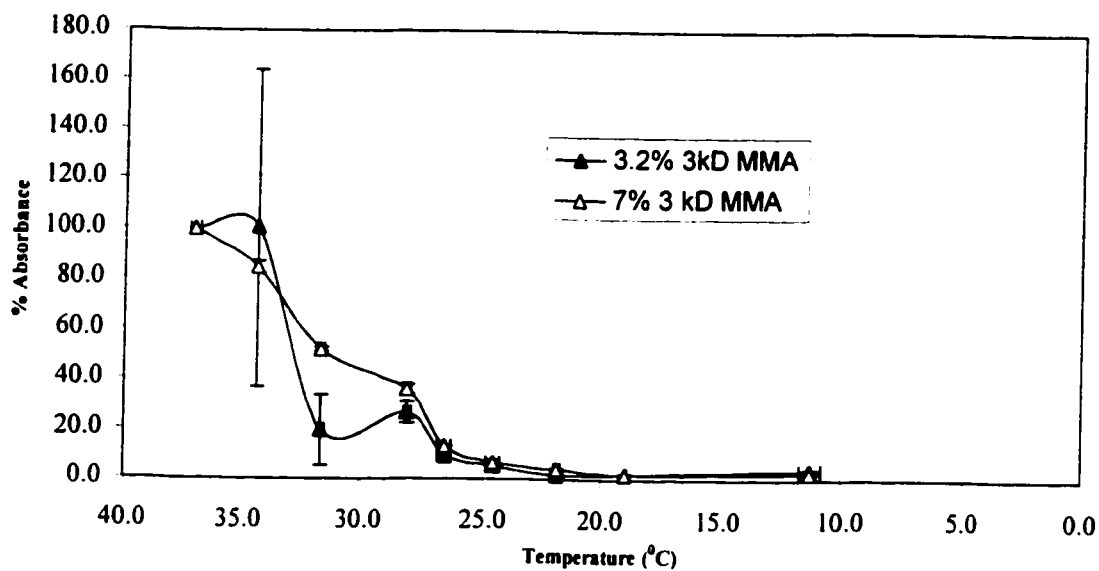


Figure 26. Degelation of low MW CP with different amount of MMA (CP8 and CP9, respectively). Where indicated, the results are mean \pm standard deviation of two samples. As the temperature was lowered, the % absorbance was reduced, until polymer was totally dissolved. At this point, % absorbance was 5%. The low MW polymer with different amount of 3 kD MMA branches exhibited similar resiliency to dissolution, even though one of the polymer had higher % of MMA.

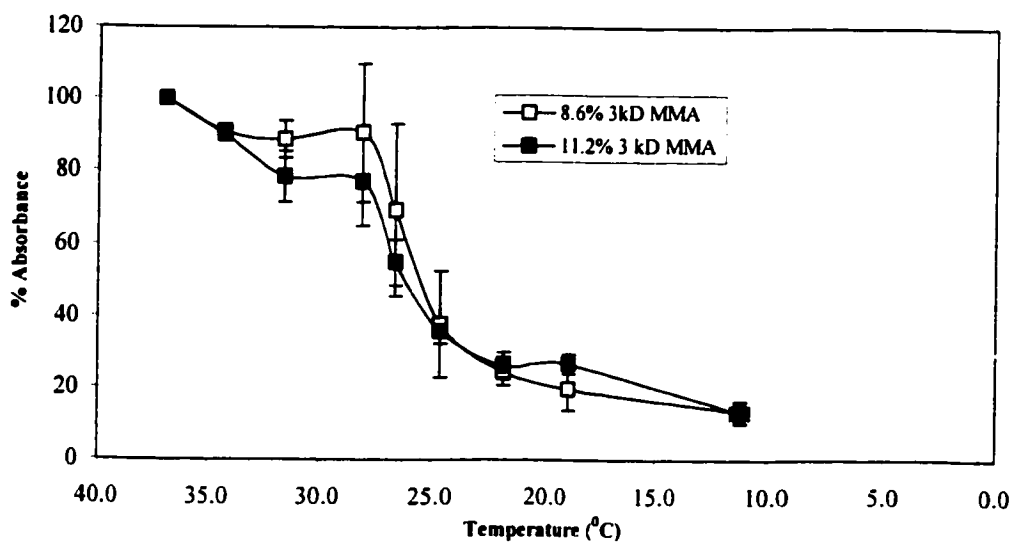


Figure 27. Degelation of high MW CP with different amount of MMA (CP11 and CP12, respectively). Where indicated, the results are mean \pm standard deviation of two samples. As the temperature was lowered, the % absorbance was reduced, until polymer was totally dissolved. At this point, % absorbance was 15%. The higher MW polymer with different amount of 3 kD MMA branches exhibited similar resiliency to dissolution, even though one of the polymers had higher % of MMA.

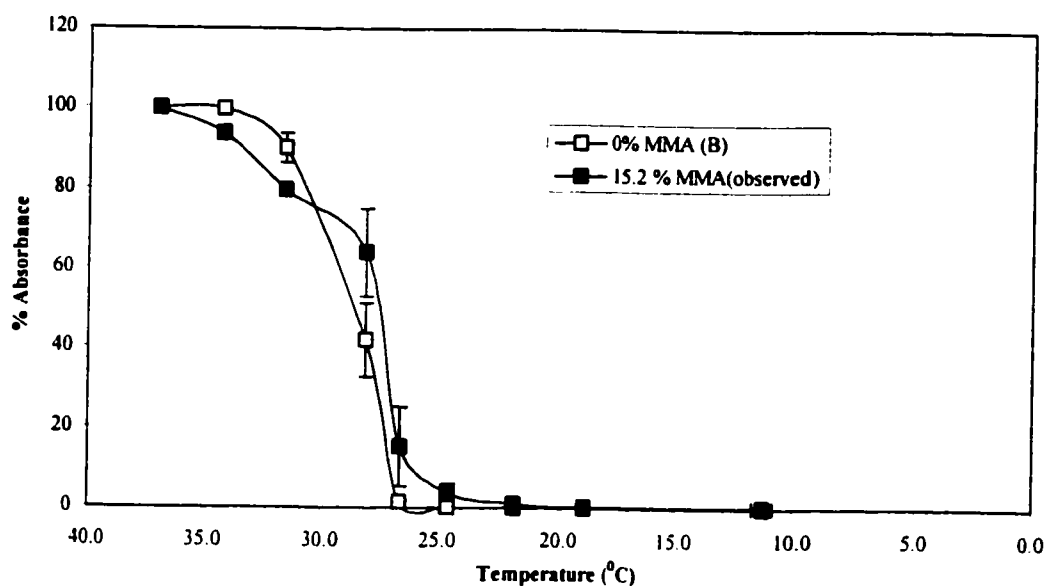


Figure 28. Degelation of high MW RP with different amount of MMA (RP5 and RP6, respectively). Where indicated, the results are mean \pm standard deviation of two samples. As the temperature was lowered, the % absorbance was reduced, until polymer was totally dissolved. At this point, % absorbance was 0. The higher MW RPs with and without MMA exhibited similar resiliency to dissolution, as evident by the need for a similar temperature to initiate dissolution. Low MW RPs failed to form gel at 37 °C.

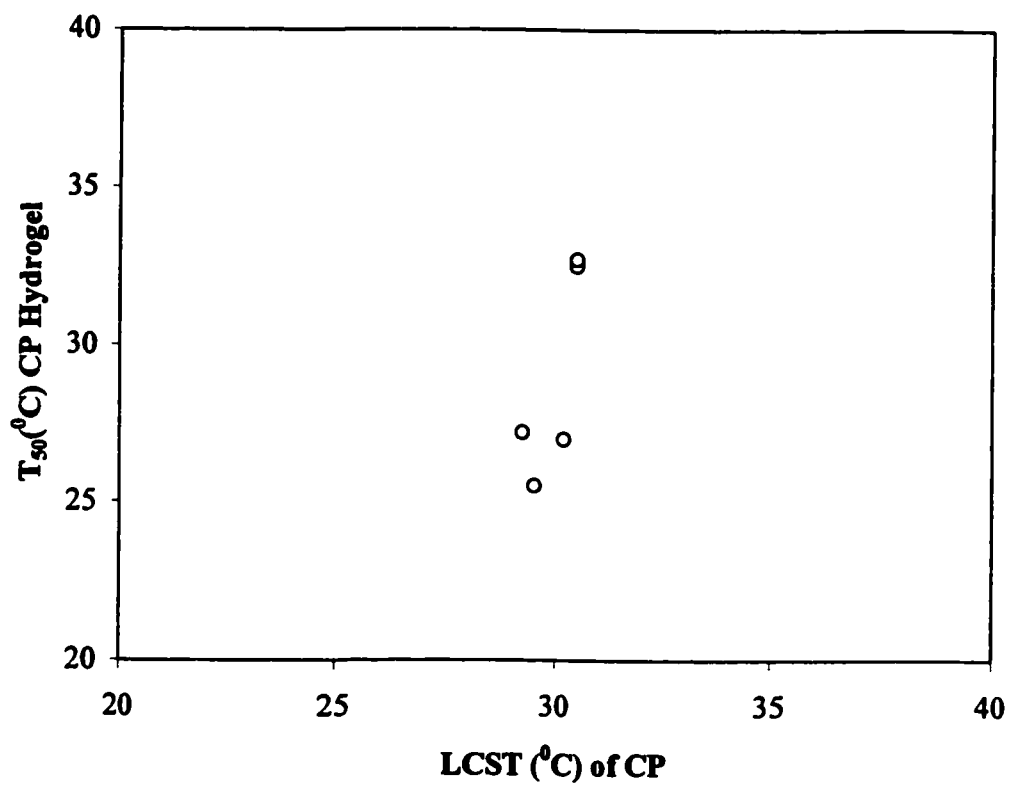


Figure 29. T₅₀ of CP hydrogels as a function of their LCST.

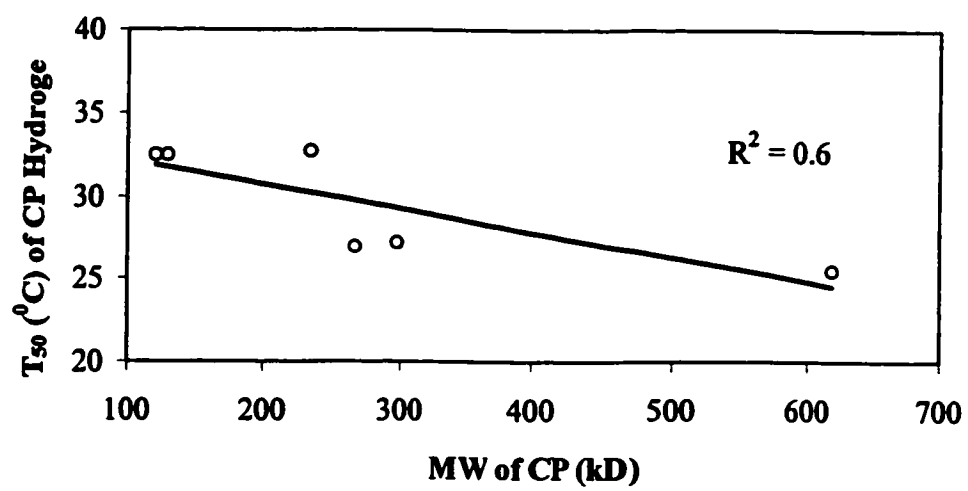


Figure 30. T_{50} of CP hydrogels as a function of their MW.

Protein Conjugation

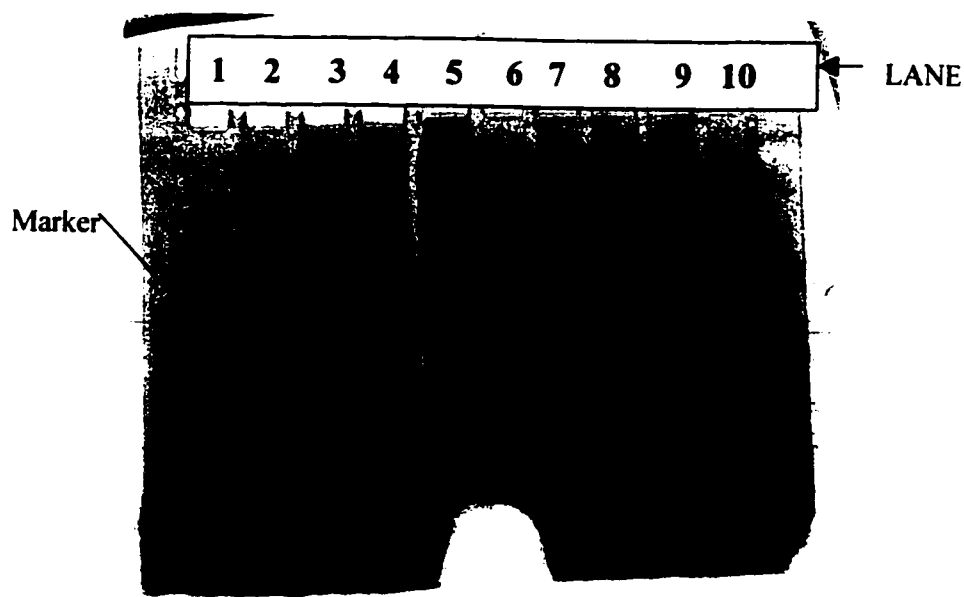
BSA Conjugation to Polymer: A Qualitative Study

BSA was conjugated to RP7 and CP14. Their LCST and composition are given in Table 18.

Table 18. Physical characteristics of RP and CP that were reacted with BSA.

Polymer	Solvent	Observed MMA in polymer (mol %)	LCST (°C)	[Succinimide] (mmol/mg polymer) X 10⁻⁶
RP7	dioxane	6.5	27	3.6
CP14	dioxane	4.5	27.9	4.9

Figure 31 shows the SDS-PAGE gel. For RP7 and CP14, a concentration dependent increase in protein conjugation was observed. No significant changes in native BSA band were observed when both polymer concentrations were 18 and 37 mg/ml. A significant reduction of native BSA band was visible when both polymer concentrations were 56 mg/ml. This suggests that MW of BSA increased because of polymer conjugation to protein. No conjugation was observed in the presence of ethanolamine. Ethanolamine aminolyzes the terminal NHS group of RP7 and CP14, so NHS group is not available for protein conjugation.



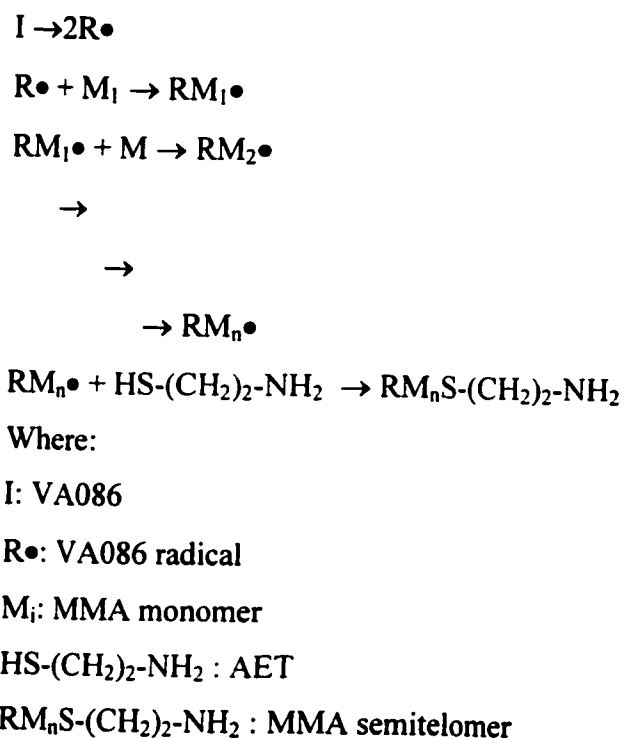
Lane	[BSA] (mg/mL)	Polymer	NiPAM/MMA (mol %)	[Polymer] (mg/mL)	LCST (°C)	[Succinimide] (mmol/mg polymer) X 10 ⁻⁶	Presence of Ethanolamine
1	-	none	-	-	-	-	no
2	1	none	-	-	-	-	no
3	1	RP7	93.5/6.5	18	27	3.6	no
4	1	RP7	93.5/6.5	37	27	3.6	no
5	1	RP7	93.5/6.5	56	27	3.6	no
6	1	RP7	93.5/6.5	56	27	3.6	yes
7	1	CP14	96.5/4.5	18	27.9	4.9	no
8	1	CP14	96.5/4.5	37	27.9	4.9	no
9	1	CP14	96.5/4.5	56	27.9	4.9	no
10	1	CP14	96.5/4.5	56	27.9	4.9	yes

Figure 31. SDS-PAGE analysis of BSA reaction with polymer RP7 and CP14. Lane 1 contained a MW marker (MW range: 15,000 D – 110,000 D). Lane 2 contained BSA alone, while other lanes contained BSA with a particular polymer. In lane 3-5, concentration of RP7 was increased from 18-56 mg/ml. In lane 7-9, concentration of CP14 was increased from 18-56 mg/ml. A gradual disappearance of BSA was observed in these lanes as the polymer concentration was increased. In lane 6, BSA band reappeared in the presence of ethanolamine even though RP7 concentration was 56 mg/ml. For CP14, this step was repeated with similar result (lane 10).

DISCUSSION

Free Radical Polymerization

A free radical polymerization is initiated by free radicals that have been produced by the decomposition of suitable free radical forming agents. In the case of thermally decomposed initiators, the covalent bonds of these agents usually break homolytically to form stable free radicals at elevated temperatures. For this project, VA086 or A501 was used as the free radical forming agent because their azo bond underwent homolytic cleavage and generated free radicals. VA086 was used to synthesize MMA semitelomer. It required 128.0 kJ/mol activation energy and had a 10 hour half-life at 86 °C (WAKO chemicals). AET was used as the chain-terminating agent (chain transfer agent). Since AET reacts with the NHS of A501, VA086 with –OH end was used. The following scheme illustrates the MMA telomerization process using VA086 and AET:



Scheme 1. Telomerization of MMA using AET as chain transfer agent.

Others have synthesized monofunctional primary amino-terminated MMA semitelomer using the free radical polymerization technique and AET [De Boos 1973; Kaneko et al. 1995]. They found that the number average MW of amino-terminated MMA semitelomer decreases with the increase in AET concentration. We found that the same relationship was true in our case. The relationship is illustrated in Figure 10. Chung and coworkers measured the MW of semitelechelic MMA-NH₂ using gel-permeation chromatography (GPC) and by titrating terminal amines (titrated with 0.05 N HClO₄ in CH₃COOH at 4 °C under N₂ atmosphere) [1997, 1998]. The MW of semitelechelic MMA-NH₂ determined using GPC was in good agreement with that determined by the end-group assay. This indicates that each semitelechelic MMA carries one amino end group.

A501 was used as an initiator to yield RP and CP with terminal succinimide group, so they are suitable for protein conjugation. A501 was synthesized in house by modifying V501 using carbodiimide chemistry [Yang et al. 2000]. The decomposition kinetics of A501 was found to be unaffected by the succinimide derivatization (at 70 °C in DMF $t_{1/2}$ (V501): 231 minutes and $t_{1/2}$ (A501): 247 minutes). Yang and coworkers found that the weight average MW of NiPAM-MMA RP is sensitive to the initiator concentration and the choice of the solvent [2000]. The initiator concentration was kept constant (0.1 mol %), so the effect of the solvent on the weight average MW of RP and CP could be studied. Two different solvents—dioxane and benzene—were used to synthesize RP and CP. Like Yang and coworkers [2000], it was found that the weight average MW of CP and RP was depended on the chain transfer efficiency of the chosen solvents. The following equation illustrates this relationship:

$$v = r_p/r_t \quad (10)$$

where:

v: degree of polymerization

r_p : rate of monomer addition to growing chains

r_t : rate of termination

The rate of monomer addition depends on the monomers. Since, for this project, all of the polymerizations were carried out using NiPAM and MMA, r_p can be considered constant. The rate of termination is dependent on the chain transfer constants of solvents. The chain transfer constant of benzene is 21×10^4 (80 °C) and dioxane is 49.1×10^4 (70 °C) [Berger and Brandrup 1989]. Hence, dioxane, in comparison with benzene, increases chain transfer reactions during polymerization. As a result, polymers that are being synthesized in benzene have lower r_t than that in dioxane. Therefore, polymers that are being synthesized in benzene have a higher MW than the polymers that are synthesized in dioxane. We found that this was true for the CP and RP that we synthesized in benzene and dioxane (see Figures 12 and 16, respectively). Han and Bae [1998], and Vernon and Coworker [2000] have also found that the NiPAM-AAc RP synthesized in benzene exhibits higher MW than that in dioxane.

N-Terminal Reactivity

Cline and Hanna [1987] used twelve amines with substantial differences in basicity and steric environment around $-\text{NH}_2$ to study the aminolysis of unsubstituted NHS esters in anhydrous dioxane solution. The pK_a of the amine ranged from 4.6 to 10.98. To study the steric environment around N, they used primary and secondary amines. The amines, which encompassed a basicity range of 6.5 pK units, displayed a 10,000-fold variation in reactivity in their reaction with the $p\text{-NO}_2$ NHS ester. As a result, for the sterically unhindered amines, they obtained a linear plot of $\log k_{\text{obsd}}$ as a function of pK_a . In other words, they found that the rate of aminolysis of NHS ester by sterically unhindered amine increased with the increase in the pK_a of the amines. Their data fitted a model in which the aminolysis proceeded through a tetrahedral intermediate model, followed by the rate-determining breakdown to products. For sterically hindered amines, such as α -methylbenzylamine and diethylamine, they found that the rate of aminolysis is much slower because of the crowding during the tetrahedral intermediate formation. Also, since there was a negative charge development on the acyl group during the transition state, they also found that the rate of aminolysis increases with the decrease in electron density at the acyl carbon.

Cline and Hanna [1988] also reported kinetic parameters with regard to the aminolysis of anisoyl-NHS ester by aliphatic amines in aqueous dioxane media. They found that the aliphatic amines with pK_a range between 7.6 and 11.1 follows a pseudo first order rate expression:

$$k_{obs} = k_{hyd} + k_{am}[amine]_{free} \quad (11)$$

where the observed rate of reaction (k_{obs}) is composed of aminolysis (k_{am}) and hydrolysis (k_{hyd}) rate constants.

For this project, semitelechelic MMA macromonomer was obtained by reacting amino-terminated semitelechelic MMA with NHS ester, such as NASI. NASI aminolysis rate was determined as outlined in Materials and Method. It was assumed that the amine of semitelechelic MMA-NH₂ reacted similar way as the small amines did, so it was expected that the semitelechelic MMA-NH₂ would follow a pseudo-first order kinetic in 50/50 MeOH/CH₃CN during reaction with NASI. Using the SWIFT kinetic software, k_{obsd} for 6 and 3 kD semitelechelic MMA-NH₂ was obtained. Figure 8 shows that the k_{obsd} increased linearly with the increase in amine concentration. k_{am} was calculated from the slopes of Figure 8. Because of higher MW, we expected that the terminal amines of 6 kD semitelechelic MMA-NH₂ would be more sterically hindered than the terminal amines of 3 kD semitelechelic MMA-NH₂. We found that the k_{am} of 6 kD MMA-NH₂ was 85% of k_{am} of 3 kD MMA-NH₂. However, we found that the difference was not statistically significant. Therefore, for our case, the MW of amino terminated semitelechelic MMA did not affect the aminolysis rate of the terminal amine. However, like Hanna and Cline (1987), we found that the decrease in electron density of acyl carbon increased the efficiency of the amide condensation reaction between semitelechelic MMA-NH₂ and carboxylic ester. As a result, amide condensation reaction between 4 kD semitelechelic MMA-NH₂ and AcCl was more efficient than the reaction between MMA-NH₂ and NASI (see Figure 9).

NHS esters have been proven to be useful acylation agents of amino acids, enzymes [Ding et al. 1997], proteins [Hoffman et al. 2000], and other compounds of biochemical interests because the lysine amino groups of protein or enzyme react with NHS esters. A significant drawback of this technique is that it can destroy the protein or enzyme's activity if the amine groups (or lysine) are critical for the protein/enzyme activity. Matsukata and coworkers have found that the molecular architecture of poly NiPAM/trypsin conjugates affect trypsin's enzymatic property [1996]. For their study, they prepared two types of NiPAM polymers: NiPAM polymers with terminal succinimide group (terminal carboxylic acid group was converted to succinimide group by reacting the carboxylic acid with NHS) and NiPAM backbone with randomly distributed succinimide groups. The following figure schematically illustrates these two types of Poly NiPAM/trypsin conjugates.

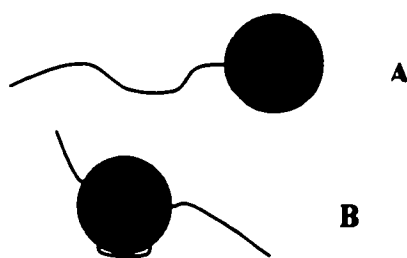


Figure 32. A: Trypsin conjugation to Poly NiPAM using single end chemistry. B: using multipoint chemistry.

Matsukata and coworkers found that when the temperature was changed across the polymer-enzyme conjugates' LCSTs in a cyclic manner, single point conjugate maintained the trypsin's enzymatic activity, whereas multipoint conjugate did not [1996]. Moreover, Ding and coworkers found that single point attachment of poly-NiPAM to trypsin improved trypsin's enzymatic activity [1998]. These studies suggest that NiPAM polymers with terminal NHS avoid multiple site modification of enzyme and therefore does not increase the chances of altering enzyme activity. Single point attachment also minimizes the blockage of enzyme's active site. Due to these findings,

we used the initiator A501 to yield end-functionalized RP and CP that have the capacity for protein conjugation.

In Phase III, we conjugated end-functionalized RP7 and CP14 to BSA. We observed the BSA conjugation by observing the gradual disappearance of BSA bands on SDS-PAGE gel as the concentration of the polymer was increased. No conjugation was observed in the presence of ethanolamine (lane 6 and 10 of Figure 10A) because it aminolyzes the terminal NHS, so NHS was not available for protein conjugation. This indicates that chemical conjugation rather than physical entrapment was the cause of BSA retention.

CP vs. RP

The phase separation behavior of homo NiPAM polymer, as well as its copolymers in aqueous solution has been investigated in the literature by a wide variety of experimental techniques, including static and dynamic laser light scattering, fluorescence, calorimetry, and visual observation of macroscopic phase separation. Wang and coworkers have studied individual monodisperse ($M_w/M_n < 1.05$) high molar mass ($M_w = 130$ MD) NiPAM polymer using static and dynamic light scattering techniques [1998]. They found that the homo NiPAM polymer went through four thermodynamically stable states across the LCST temperature. Below LCST, NiPAM chain existed in a well-hydrated “coil” state. At the LCST, NiPAM chain existed in two thermodynamically stable states: “crumpled coil” and “molten globule.” Above LCST, it existed in a “globule” state while retaining 66 % water. Solution calorimetry provided thermodynamic parameters that lent insight into the forces responsible for the NiPAM polymer phase separation and measured transition enthalpies that was consistent with the loss of approximately one hydrogen bond per NiPAM repeating unit [Schild and Tirrell 1990; Otake et al. 1990]. In the “coil” state, relatively strong hydrogen bonds formed between water molecules and N-H and C=O groups of NiPAM polymer. As the temperature was raised, these hydrogen bonds became weaker, which resulted in an endothermic heat of phase separation. This led to “crumpled coil” and “molten globule” state. These states were followed by the formation of polymer

aggregates through interpolymeric hydrogen bonding, which led to “globule” state. Knowledge about the behaviour of the homo NiPAM has been used to change the LCST of NiPAM polymer. The LCST of NiPAM polymer has been manipulated by copolymerizing NiPAM with randomly distributed hydrophilic [Feil et al. 1993] and hydrophobic monomers [Uludag et al. 2001]. Feil and coworkers concluded that hydrophilic comonomers increase NiPAM polymer’s LCST by increasing its hydrophilicity, whereas hydrophobic comonomers does the opposite [1993]. We observed the similar trend with our NiPAM-AAc-MMA RP. That is, hydrophobic monomer MMA decreased the LCST of NiPAM-AAc-MMA RP (shown in Figure 18). MMA composition of the RP was dependent on the MMA feed ratios during polymerization (shown in Figure 17). Since, AAc content was kept constant at 2 mol %, a correlation between the LCST of NiPAM-AAc-MMA polymers and AAc content was not clearly demonstrated (shown in Figure 15). Incorporating AAc, however, made the polymers soluble hence AAc increased the overall solubility.

CPs have been found to behave differently than the RPs. Ringsdorf and coworkers synthesized pyrene labeled hydrophobically modified NiPAM CP [1991]. They found that the LCST of NiPAM CP decreased for CP containing C_{10} and C_{14} alkyl chains. Surprisingly, this trend was reversed in the C_{18} containing copolymers: they had an LCST lower than homo NiPAM polymer but higher than the C_{14} containing copolymers. Using fluorescence techniques and fluorescent labeled CP, Ringsdorf and coworkers found that, below LCST, hydrophobically modified NiPAM CP has a highly viscous hydrophobic core and a loose corona [Ringsdorf et al. 1992]. This suggests that the longer alkyl chains ($>C_{17}$) are not exposed to water but rather form a micellar structure protected from the water and therefore do not make a hydrophobic contribution to the LCST. We observed a similar trend. Hydrophobic semitelechelic MMA macromonomer failed to change the LCST of NiPAM-AAc-MMA CP (shown in Figure 14). In contrast to RP, MMA content of CP was generally lower than the feed ratio (shown in Figure 13) because MMA macromonomer is more difficult to incorporate in the polymer than MMA monomers. Since, AAc content was kept constant, LCST of CP was not affected by AAc (shown in Figure 11).

In another study, Ringsdorf and coworkers found that above LCST the micellar structure of NiPAM-alkylacrylamide (C_{18}) CP was disrupted severely [Ringsdorf et al 1992] and the polymers became entangled. Chung and coworkers found that CP of NiPAM-methacrylic acid stearyl ester (MASE) (length of carbon chain: C_{18}) become increasingly entangled during heating/cooling cycle across the LCST [1998]. As a result, micellar size increases at each heating/cooling cycle. We hoped that this interpolymeric aggregation of CP would allow us to synthesize more stable gels than the gels of RP. Using free pyrene and fluorescence technique, Ringsdorf and coworkers also found that the rigidity of hydrophobic core of NiPAM-alkylacrylamide CP micelle increases as a function of alkyl chain length. It was thought that this would translate into improved CP gel stability. Hence, we synthesized CP with different alkyl chain lengths. MWs of MMA side chain were 3 kD, 6 kD, and 10 kD.

For our gel study (hydrogel dissolution approach), we determined gel stability as the driving force for dissolution became stronger. Through the LCST study, we knew the polymers display propensity to form a cohesive gel as they lose water-solubility below the physiological temperature. Degelation study was carried out to determine the stability of these hydrogels. The degelation was monitored by measuring the absorbance of the gel. The dissolution force was increased by decreasing the gel temperature below the LCST. We found that the length of NiPAM-AAc backbone and molecular architecture were crucial for gel stability, not the length of MMA side chain or MMA content because: (i) low MW random polymer did not gel (not shown), whereas high MW random polymers did (Figure 28); (ii) high MW CP formed more stable gel than low MW CP regardless of the length of MMA side chain (Figures 21-23); (iii) longer MMA side chain failed to improve the gel stability when the MW of polymer were similar (Figures 24-25). This is in contrast to the studies that were mentioned above. Our result is unique because our CPs have hydrophobic chains that are > 3 kD instead of only 18 carbon long. It is likely that above 3 kD, the effect of MMA chain length on gel stability become ineffective; (iv) given the limited range of MMA composition of CP, increasing amount of MMA failed to improve the gel stability when the MW of polymer were similar (Figures 26-27).

Moreover, T_{50} of CP is independent of the CPs LCST. This makes sense because above LCST CPs become entangled, and the gel stability depends on the degree of micelle aggregation. In contrast, T_{50} of high MW RP is dependent on the LCST because above LCST, RPs have the propensity to form a cohesive gel but the polymer chains do not become sufficiently entangled; therefore, gel stability of RP is related to its LCST.

CONCLUSIONS

Following conclusions can be drawn from this thesis:

- (1) A methodology was developed to synthesize temperature-sensitive polymers based on N-isopropylacrylamide with controlled architecture.
- (2) Comb polymers were synthesized by using a semitelechelic methylmethacrylate macromonomer, which was prepared by reacting an amine-terminated semitelechelic methylmethacrylate with acryloylchloride. Acrylic acid in the backbone was necessary for polymer solubility.
- (3) LCST changed with mol% of methylmethacrylate for random polymer, but for comb-type polymer there was no effect of methylmethacrylate graft mol% on LCST.
- (4) We found LCST of random polymer decreased with the increase in methylmethacrylate content of the polymer.
- (5) In contrast, LCST of comb-type polymer remained unaffected by the increase in methylmethacrylate content. The length of the side-chain did not affect the LCST.
- (6) Polymers formed gels and in general high MW polymers were more amenable to gelation. Chain-chain entanglements are likely to contribute to gel stability.
- (7) Low MW comb-type polymer did form gel (unlike random polymer).
- (8) Gel stability of comb-type polymer was not dependent on the methylmethacrylate chain length, which was between 3 and 10 kD. The critical chain length, if any, may be lower than 3 KD and remains to be determined.
- (9) We did a qualitative protein conjugation study where Albumin was conjugated to NHS-terminal end of RP7 and CP14. This showed that the end-functionalized polymers are capable of conjugating to protein.
- (10) Overall results from this thesis point out to the possibility of controlling and engineering temperature sensitive polymer properties.
- (11) In the future, these polymers will be useful in developing an “open” vehicle for graft transplantation.

FUTURE DIRECTIONS

This thesis gave promising result in controlling polymer properties for specific use. However, further investigation is required in the following aspects:

Polymer Architecture. Others have found that the rigidity of hydrophobic core of NiPAM-alkylacrylamide CP micelle increased as a function of alkyl chain length [Ringsdorf et. al. 1992]. For this project, longer (> 3kD) MMA side chain failed to improve the gel stability. This is may be due to critical MMA side chain length. Beyond this length, MMA side chain becomes ineffective for improving gel stability. In the future, smaller (< 3 kD) MMA side chains can be synthesized by increasing the concentration of AET. CPs with small MMA side chains will allow us to determine the MW of critical chain length. Also, longer MMA side chains make CP insoluble. For this project, hydrophilic monomer AAc was added to improve polymer solubility. Smaller MMA side chains would avoid this complication.

Protein Conjugation. End-functionalized polymers with terminal NHS reduce the chances of altering protein activity. Single point attachment also minimizes the blockage of protein's active site. In this project, we obtained the end-functionalized polymers by preparing a free radical initiator with protein reactive succinimide ends and using it during thermal polymerization process. We found that the end-functionalized polymers conjugate to BSA. In the future, the possibility of conjugating end-functionalized polymers to immunosuppressive proteins needs to be explored. Other studied, can also be designed to determine the following aspects: (i) the critical concentration of polymer at which 50% of the protein binds to polymer in 24 and 48 hours incubation period, (ii) the resiliency of the chemical bond over a certain period of time, and (iii) the effect of protein conjugation on polymer's physical properties, such as LCST and gel stability.

Cell Compatibility. It is imperative that polymer-protein complex is not cytotoxic to cells or tissues (e.g. islets) and, nutrients and metabolic end-products are effectively transported through the gels. Hence, cell or tissue viability and functionality should be assessed using biochemical assays. In general, *in vitro* assays will serve as an initial screen to identify promising polymers for *in vivo* studies.

LITERATURE CITED:

- Abbas A. 1996. Die and let live: Eliminating Dangerous Lymphocytes. Cell 84:655-657.**
- Allison J., Georgiou H., Strasser A., Vaux D. 1997. Transgenic expression of CD95 ligand on islet β cells induces a granulocytic infiltration but does not confer immune privilege upon islet allografts. Proc Natl Acad Sci USA 94:3943-3947.**
- Badiger M, Lele A, Bhalerao V, Varghese S. 1998. Molecular tailoring of thermoreversible copolymer gels: some new mechanistic insights. J Chem Phys. 109: 1175-1184.**
- Balow J., Boumpas D., Austin H. 2000. New Prospects for treatment of lupus nephritis. Semin Nephrol 20:32-39.**
- Batteux F., Lores P., Bucchini D., Chiocchia G. 2000. Transgenic expression of Fas ligand on thyroid follicular cells prevents autoimmune thyroiditis. J Immunol 164:1681-1688.**
- Batteux F., Tourneur L., Trebeden H., Charreire J., Chiocchia G. 1999. Gene therapy of experimental autoimmune thyroiditis by in vivo administration of plasmid DNA coding for Fas ligand. J Immunol 162:603-608.**
- Bellgrau D, Gold D, Selawry H, Moore J, Franzusoff A, Duke RC. 1995. A role for CD95 ligand in preventing graft rejection. Nature 377:630-2.**
- Berger KC, Brandrup G. 1989. Transfer constant to monomer, polymer, catalyst, solvent, and additive in free radical polymerization. In: Brandrup J, Immergut EH, editors. Polymer Handbook (3rd edition). New York: Wiley and Son. p. II/81.**
- Calafiore R, Basta G, Osticioli L, Luca G, Tortoioli C, Brunetti P. 1996. Coherent Microcapsules for Pancreatic Islet Transplantation: A New Approach for Bioartificial Pancreas. Transplant. Proc. 28: 812-813.**

- Chen G, Hoffman AS. 1995. Graft copolymers that exhibit temperature-induced phase transitions over a wide range of pH. *Nature* 373:49-52.**
- Chen J., Sun Y., Nabel G. 1998. Regulation of the proinflammatory effects of Fas ligand (CD95L). *Science* 282:1714-1717.**
- Chung J, Yokoyama M, Aoyagi T, Sakurai Y, Okano T. 1998. Effect of molecular architecture of hydrophobically modified poly(N-isopropylacrylamide) on the formation of thermoresponsive core-shell micellar drug carriers. *J Control Rel.* 53:119-130.**
- Cline GW, Hanna SB. 1987. The aminolysis of N-hydroxysuccinimide esters. A structure-reactivity study. *J Am Chem Soc* 109:3087-3091.**
- Cline GW, Hanna SB. 1988. Structures and mechanisms of the aminolysis of N-hydroxysuccinimide esters in aqueous buffers. *J Org Chem* 53:3583-3586.**
- De Boos AG. 1973. Preparation and characterization of some polymers terminated with primary amino groups. *Polymer* 14:587-588.**
- De Mattos A., Olyaei A., Bennett W. 2000. Nephrotoxicity of immunosuppressive drugs: long-term consequences and challenges for the future. *Am J Kidney Dis* 35:333-346.**
- Ding Z, Chen G, Hoffman AS. 1998. Unusual properties of thermally sensitive oligomer-enzyme conjugates of poly(N-isopropylacrylamide)-trypsin. *J Biomed Mat Res.* 39:498-505.**
- Dixit V, Arthur M, Reinhardt R, Gitnick G. 1992. Improved function of microencapsulated hepatocytes in a hybrid bioartificial liver support system. *Artificial Organs.* 16: 336-341.**

Feil H, Bae YH, Feijen J, Kim SW. 1993. Effect of Comonomer Hydrophilicity and Ionization on the Lower Critical Temperature of N-Isopropylacrylamide Copolymers. *Macromol* 26: 2496-2500.

Garfinkel MR, Harland RC, Opara EC. 1998. Optimization of the microencapsulated islet for transplantation. *J. Surgical Research*. 76: 7-10.

Griffith TS, Brunner T, Fletcher SM, Green DR, Ferguson TA. . 1995. Fas ligand-induced apoptosis as a mechanism of immune privilege. *Science*. 270: 1189-1192.

Han CK, Bae YH. 1998. Inverse thermally-reversible gelation of aqueous N-isopropylacrylamide copolymer solutions. *Polymer* 39:2809-2814.

Hoffman AS, Stayton PS, Bulumus V, Chen G, Chen J, Cheung C, Chilkoti A, Ding Z, Dong L, Fong R, Lackey C, Long CJ, Miura M, Morris JE, Murthy N, Nabeshima Y, Park TG, Press OW, Shimoboji T, Shoemaker S, Yang HJ, Monji N, Nowinski RC, Cole CA, Priest JH, Harris JM, Nakamae K, Nishino T, Miyata T. 2000. Really smart bioconjugates of smart polymers and receptor proteins. *J Biomed Mater Res* 52:577-586.

Huglin MB. 1989. Specific refractive index increments of polymers in dilute solution. In: Brandrup J, Immergut EH, editors. *Polymer Handbook* (3rd edition). New York: Wiley and Son. p. VII/409-VII/411.

Judge T., Desai N., Yang Z., Rostami S., Alonso L., Zhang H., Chen Y., Markman J., Demateo R., Barker C., Naji A., Turka L. 1998. Utility of adenoviral-mediated Fas ligand gene transfer to modulate islet allografts survival. *Transplantation* 66(4):426-434.

Kaneko Y, Sakai K, Kikuchi A, Yoshida R, Sakurai Y, Okano T. 1995. Influence of freely mobile grafted chain length on dynamic properties of comb-type grafted poly(N-isopropylacrylamide) hydrogels. *Macromol* 28:7717-7723.

- Kang S., Schneider D., Lin Z., Hanahan D., Dichek D., Stock P., Baekkeskov S. 1997. Fas ligand expression in islets of Langerhans does not confer immune privilege and instead targets them for rapid destruction. *Nat Med* 3(7):738-743.**
- Korbitt G., Elliot J., Rajotte R. 1997. Cotransplantation of allogenic islets with allogeneic testicular cell aggregates allows long-term graft survival without systemic immunosuppression. *Diabetes* 46:317-322.**
- Korbitt G., Surez-Pinson W., Power R., Rajotte R., Rabinovitch A. 2000. Testicular sertoli cells exert both protective and destructive effects on syngeneic islet grafts in non-obese diabetic mice. *Diabetologia* 43:474-480.**
- Lau HT, Yu M, Fontana A, Stoeckert CJ Jr. 1996. Prevention of islet allograft rejection with engineered myoblasts expressing FasL in mice. *Science* 273:109-12.**
- Lim F, Sun AM. 1980. Microencapsulated islets as bioartificial endocrine pancreas. *Science* 210:908-910.**
- Lowin B, Hahne M, Mattmann C, Tschopp J. 1994. Cytolytic T-cell cytotoxicity is mediated through perforin and Fas lytic pathways. *Nature* 370:650-2.**
- Lum ZP, Krestow M, Tai IT, Vacek I, Sun AM. 1992. Xenografts of Rat Islets into Diabetic Mice. *Transplant.* 53: 1180-1183.**
- Lum ZP, Tai IT, Krestow M, Norton J, Vacek I, Sun AM. 1991. Prolonged Reversal of Diabetic State in NOD Mice by Xenografts of Microencapsulated Rat Islets. *Diabetes.* 40: 1511-1516.**
- Matsukata M, Aoki T, Sanui K, Ogata N, Kikuchi A, Sakurai Y, Okano T. 1996. Effect of molecular architecture of poly(N-isopropylacrylamide)-trypsin conjugates on their solution and enzymatic properties. *Bioconjugate Chem* 7: 96-101.**

- Mikos AG, Papadaki MG, Kouvroutoglou S, Ishaug SL, Thomson RC. 1994. Mini-Review: Islet Transplantation to Create a Bioartificial Pancreas. *Biotechnol. Bioeng.* 43: 673-677.**
- Miron T, Wilchek M. 1982. A spectrophotometric assay for soluble and immobilized N-hydroxysuccinimide esters. *Anal Biochem.* 126:433-435.**
- Otake K, Inomata H, Konno M, Saito S. 1990. Thermal analysis of the volume phase transition with N-isopropylacrylamide gels. *Macromol.* 23:283-289.**
- Ringsdorf H, Simon J, Winnik FM. 1992. Hydrophobically-modified poly(N-isopropylacrylamides) in water: probing of the microdomain composition by nonradiative energy transfer. *Macromol.* 25:5353-5361.**
- Ringsdorf H, Simon J, Winnik FM. 1992. Hydrophobically-modified poly(N-isopropylacrylamides) in water: a look by fluorescence techniques at the heat-induced phase transition. *Macromol.* 25:7306-7312.**
- Ringsdorf H, Venzmer J, Winnik FM. 1991. Fluorescence studies of hydrophobically modified poly(N-isopropylacrylamides). *Macromol.* 24:1678-1686.**
- Shibayama M, Mizutani S, Nomura S. 1996. Thermal properties of copolymer gels containing N-isopropylacrylamide. *Macromol* 29:2019-2024.**
- Schilfgaarde RV, Vos PD. 1998. Factors in success and failure of microencapsulated pancreatic islets. *Transplant Proc* 30: 501-502.**
- Schild HG. 1991. Probes of the lower critical solution temperature of poly(N-isopropylacrylamide). In *Water-Soluble Polymers*. Washington, DC: ACS Press pp. 249-260.**
- Schild HG, Tirrell D. 1990. Microcalorimetric detection of lower critical solution temperatures in aqueous polymer solutions. *J Phys Chem.* 94:4352-4356.**

Strasser A., O'Connor L. 1998. Fas ligand-caught between Scylla and Charybdis. *Nature Medicine*. 4: 21-22.

Takeda Y., Gotoh M., Dono K., Nishihara M., Grochowiecki T., Kimura F., Yoshida T., Ohta Y., Ota H., Ohzato H., Umeshita K., Takeda T., Matsuura N., Sakon M., Kayagaki N., Yagita H., Okumura K., Miyasaka M., Monden M. 1998. Protection of islet allografts transplanted together with fas ligand expressing testicular allografts. *Diabetologia* 41:315-321.

Takeuchi T., Ueki T., Nishimatsu H., Kajiwara T., Ishida T., Jishage K., Ueda O., Suzuki H., Li B., Moriyama N., Kitamura T. 1999. Accelerated rejection of Fas ligand-expressing heart grafts. *J Immunol* 162:518-522.

Tatarkiewicz K, Sitarek E, Fiedor P, Sabat M, Orłowski T. 1994. In Vitro and In Vivo Evaluation of Protamine-Heparin Membrane for Microencapsulation of Rat Langerhans Islets. *Artificial Organs*. 18: 736-739.

Tanaka M., Suda T., Yatomi T., Nakamura N., Nagata S. 1997. Lethal effect of recombinant human Fas ligand in mice pretreated with *Propionibacterium acnes*. *J Immunol* 158:2303-2309.

Uludag H, Fan XD. 2000. Synthesis and characterization of thermoreversible, protein conjugating copolymers based on N-isopropylacrylamide. In: Park K, Msryn R, editors. *Drug delivery in the 21st century*. Washington, DC: ACS Press.

Uludag H, Norrie B, Kousinioris N, Gao T. 2001. Engineering temperature-sensitive poly(N-isopropylacrylamide) polymers as carriers of therapeutic proteins. *Biotechnol Bioeng*. 73:510-21.

Uludag H, Sefton MV. 1993. Metabolic activity and proliferation of CHO cells in hydroxyethyl methacrylate-methyl methacrylate (HEMA-MMA) microcapsules. *Cell Transplant*. 2:175-182.

Uludag H, Sefton MV. 1992. Metabolic activity of CHO fibroblasts in HEMA-MMA microcapsules. *Biotechnol. Bioeng.* 39: 672-678.

Uludag H, Vos PD, Tresco PA. 2000. Technology of mammalian cell encapsulation. *Adv Drug Deliv Rev* 42:29-74.

Uludag H, Wong M, Man J. 2000. Reactivity of temperature-sensitive, protein-conjugating polymers prepared by a photopolymerization process. *J Appl Polym Sci* 75:583-592.

Veron B. 1996. Thermally reversible polymer gels for biohybrid artificial pancreas. *Macromol Symp.* 109:155-167.

Vernon B, Kim SW, Bae YH. 2000. Thermoreversible copolymer gels for extracellular matrix. *J Biomed Mater Res* 51: 69-79.

Wang X, Qiu X, Wu C. 1998. Comparison of the coil-to-globule and the globule-to-coil transitions of a single poly(N-isopropylacrylamide) homopolymer chain in water. *Macromol* 31:2972-2976.

Weber CJ, Zabinski S, Koschitzky T, Wicker L, Rajotte R, D'Agati V, Peterson L, Norton J, Reemtsma K. 1990. The role of CD4+ helper T cells in the destruction of microencapsulated islet xenografts in nod mice. *Transplant* 49:396-404.

Yang J, Singh P, Somayaji V, Uludag H. 2000. Functional polymers for protein conjugation at a single site. Submitted to *Bioconjugate Chem.*

Yao Q., Glorioso J., Evans C., Robbins P., Kovesdi I., Oligino T., and Ghivizzani S. 2000. Adenoviral mediated delivery of Fas ligand to arthritic joints causes extensive apoptosis in the synovial lining. *J Gene Med* 2:210-219.

Zekorn TD, Horcher A, Mellert J, Siebers U, Altug T, Emre A, Hahn HJ, Federlin K. 1996. Biocompatibility and immunology in the encapsulation of islets of Langerhans (bioartificial pancreas). *Int J Artif Organs* 19:251-7.

Zhang H., Yang Y., Horton J., Samoilova E., Judge T., Turka L., Wilson J., Chen Y. 1997. Amelioration of collagen-induced arthritis by CD95 (APO-1/Fas)-ligand gene transfer. J Clin Invest 100:1951-1957.

Zhou S, Fan S, Au-yeung S, Wu C. 1995. Light-scattering studies of poly(N-isopropylacrylamide) in tetrahydrofuran and aqueous solution. Polymer 36(7):1341-1346.

Appendix A

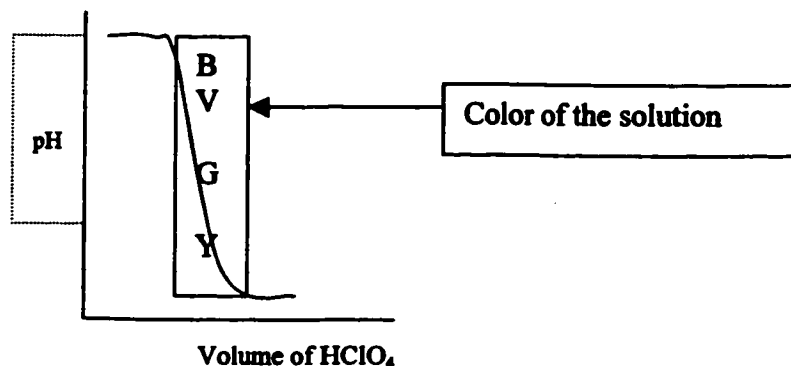


Figure 33. A theoretical titration curve for amino terminated semitelechelic MMA. BV: blue-violet; G: green; Y: yellow.

Volume of HClO ₄ (μL)	Color of the solution
100	Violet
200	Violet
300	Violet
350	Blue
360	Blue-green (neutralization point)
370	Green

Table 19. Titration of amino terminated (14 % AET) semitelechelic MMA.

$$\begin{aligned}
 n_1 &= n_2 = C \times V \\
 &= (0.1 \text{ M}) (3.6 \times 10^{-4} \text{ L}) \\
 &= 3.6 \times 10^{-5} \text{ mol of semitelechelic MMA-NH}_2.
 \end{aligned}$$

where:

n_1 = moles of HClO₄.

n_2 = moles of semitelechelic MMA-NH₂.

C = Concentration of HClO₄.

V = Volume of HClO₄ added till neutralization point.

$$\begin{aligned}
 \text{MW} &= m / n \\
 &= 0.1 \text{ g} / 3.6 \times 10^{-5} \text{ mol} \\
 &= 2777 \text{ g/mol} \\
 &= 3 \text{ kD.}
 \end{aligned}$$

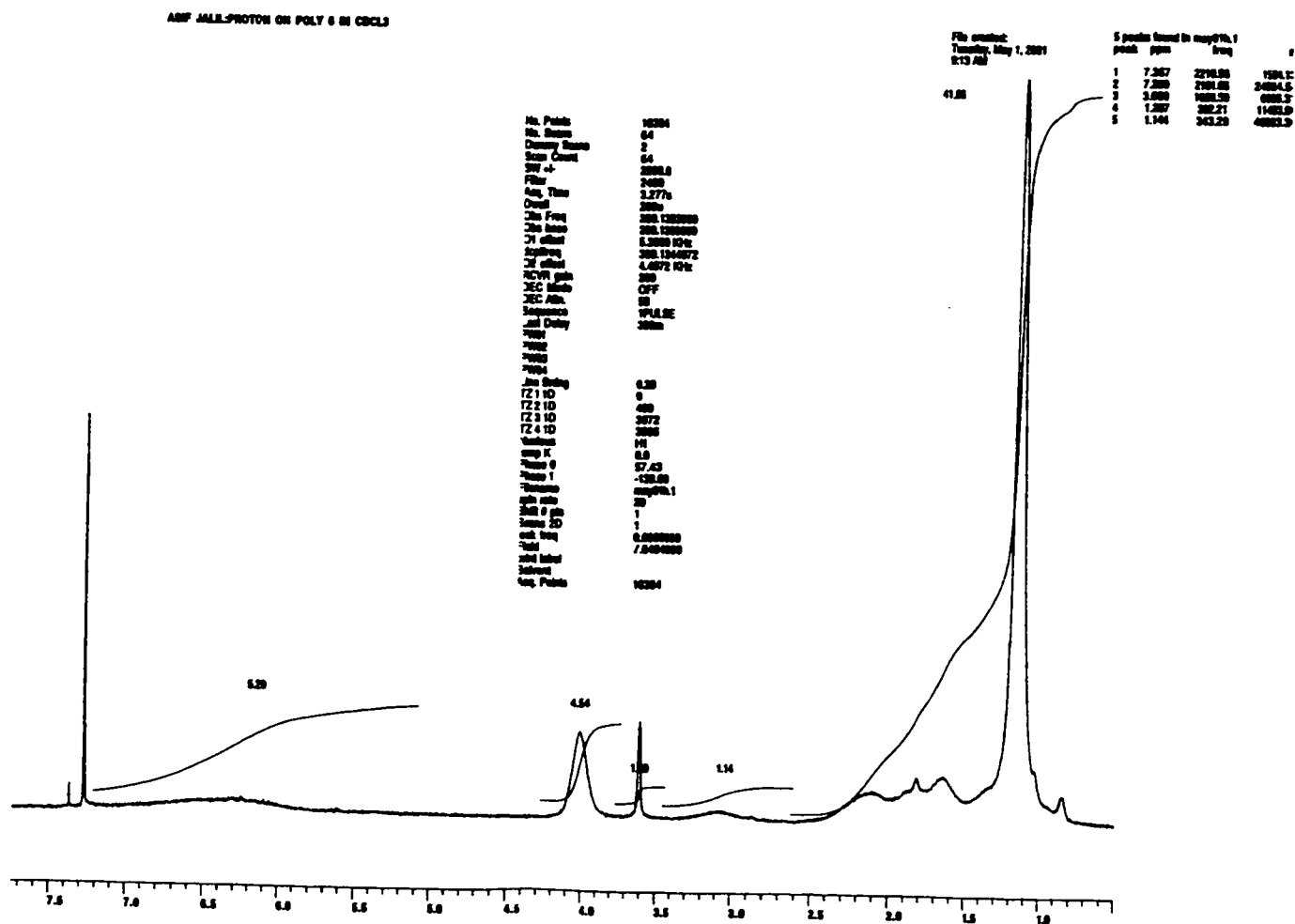
where:

MW = MW of semitelechelic MMA-NH₂.

m = mass of semitelechelic MMA-NH₂ sample.

n = moles of semitelechelic MMA-NH₂ in sample.

Appendix B



NMR spectrum of CP6. For MMA, the peak area is determined by three hydrogens, the normalized peak area is $1.00/3$, which is 0.33 . Total peak area is $4.54 + 0.33 = 4.87$. NiPAM content is $(4.54/4.87) \times 98\% = 92\%$. MMA content is $(0.33/4.87) \times 98\% = 6\%$. The NiPAM and MMA content of this particular polymer was multiplied by 98.1% because the polymer had 2.0% AAC. AAC content was determined using titration.

Appendix C

NaOH added (μL)	Color of the Solution
35	Colorless
50	Colorless
200	Colorless
1000	Colorless
1400	Pink
1420	Pink
1440	Pink (neutralization point)
1462	Red
1502	Red

Table 20. Amount of NaOH was added to neutralize AAc of a particular polymer.

$$\begin{aligned}
 n_1 \text{ of NaOH} &= n_2 \text{ of AAc} \\
 &= C \times V \\
 &= 0.01 \text{ M} \times 1.44 \times 10^{-3} \text{ L} \\
 &= 1.44 \times 10^{-5} \text{ mol of AAc.}
 \end{aligned}$$

where:

n_1 = mol of NaOH at the neutralization point.

n_2 = mol of AAc.

C = Concentration of NaOH.

V = Amount of NaOH that was added until neutralization point.

$$\begin{aligned}
 m &= n \times \text{FW} \\
 &= 1.44 \times 10^{-5} \text{ mol} \times 72.06 \text{ g/mol} \\
 &= 0.001 \text{ g.}
 \end{aligned}$$

where:

m = mass of AAc.

n = moles of AAc.

FW = molecular weight of AAc.

$$\begin{aligned}
 \% \text{ mass ratio of AAc} &= (m_1/m_2) \times 100 \% \\
 &= (0.001 \text{ g} / 0.056 \text{ g}) \times 100 \% \\
 &= 1.8 \%.
 \end{aligned}$$

where:

m_1 = mass of AAc.

m_2 = mass of polymer sample.

Appendix D

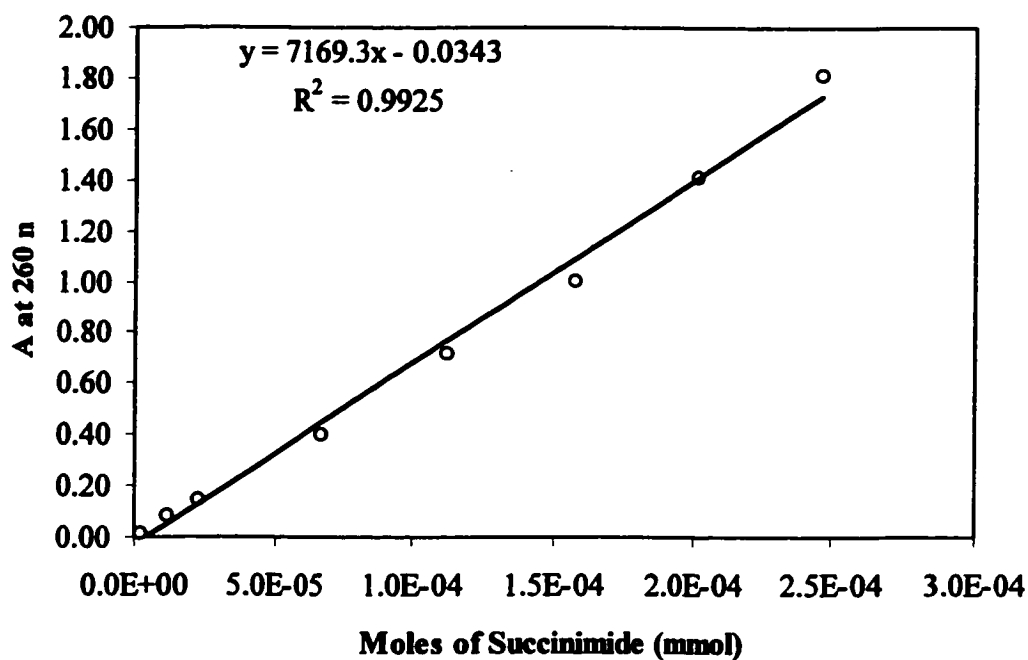


Figure 34. Succinimide Calibration Curve.

$$\begin{aligned}\text{mmol of succinimide} &= (A + 0.0343) / 7169.3 \\ &= (1.2 + 0.0343) / 7169.3 \\ &= 1.7 \times 10^{-4}\end{aligned}$$

$$\begin{aligned}[\text{Succinimide}] &= \text{mmol of succinimide} / \text{mass of polymer sample} \\ &= 1.7 \times 10^{-4} \text{ mmol} / 10 \text{ mg} \\ &= 1.7 \times 10^{-5} \text{ mmol/mg}\end{aligned}$$

Appendix E

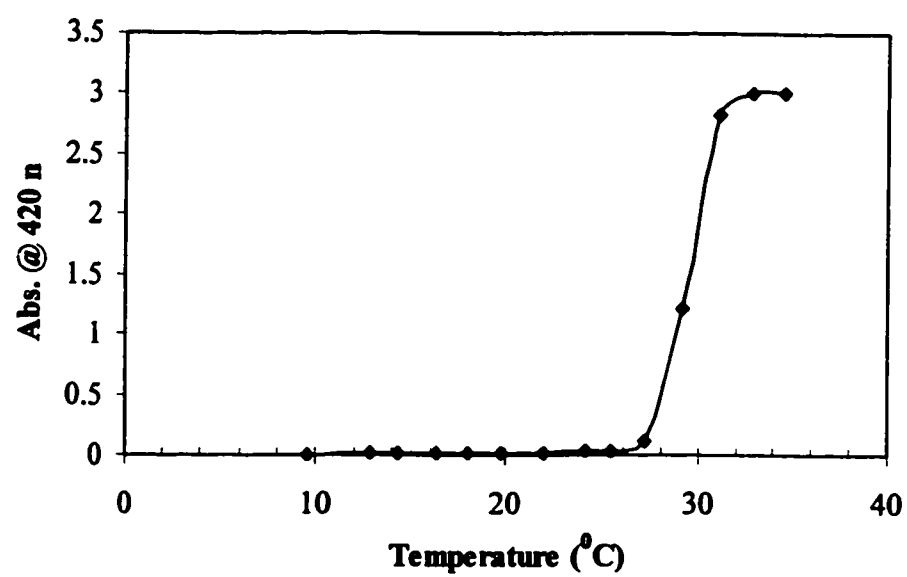


Figure 35. LCST of NiPAM polymer that was synthesized in benzene.

Appendix F

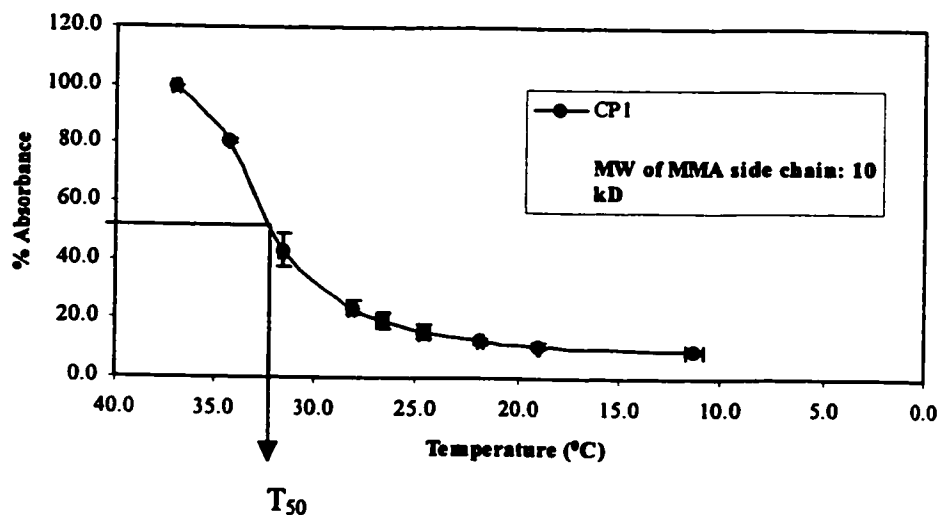


Figure 36. Hydrogel dissolution curve of CP1.

Temp (°C)	Abs	Temp _{avg} (°C)	SD	% Absorbance	Average % Absorbance	SD
37.1	1.856	37.0	0.2	100.0	100.0	0.0
36.8	1.679	34.3	0	100.0	80.8	0.6
34.3	1.507	31.6	0.1	81.2	43.4	5.8
34.3	1.349	28.1	0.1	80.3	23.9	2.3
31.7	0.881	26.6	0.3	47.5	19.6	2.8
31.5	0.659	24.6	0.3	39.2	15.8	2.4
28	0.413	21.9	0.1	22.3	12.6	0.9
28.2	0.429	19.0	0.1	25.6	11.1	1.1
26.4	0.328	11.2	0.4	17.7	9.6	0.8
26.8	0.363			21.6		
24.4	0.262			14.1		
24.8	0.293			17.5		
22	0.245			13.2		
21.8	0.2			11.9		
19	0.191			10.3		
18.9	0.199			11.9		
10.9	0.169			9.1		
11.5	0.171			10.2		

Table 21. Raw data for CP1 degelation study. Samples were in duplicate. SD is standard deviation. Temp is temperature.

Since the samples were in duplicate, both absorbencies at 37 °C were considered 100 %.

% Absorbance was calculated as follow:

For the sample

$$\begin{aligned}\% \text{ Absorbance} &= (\text{absorbance at } 34.3 \text{ }^{\circ}\text{C} / \text{absorbance at } 37.1 \text{ }^{\circ}\text{C}) \times 100\% \\ &= (1.507/1.856) \times 100\% \\ &= 81 \%\end{aligned}$$

For its duplicate

$$\begin{aligned}\% \text{ Absorbance} &= (\text{absorbance at } 34.3 \text{ }^{\circ}\text{C} / \text{absorbance at } 36.8 \text{ }^{\circ}\text{C}) \times 100\% \\ &= (1.349/1.679) \times 100\% \\ &= 80 \%\end{aligned}$$

The % absorbance of the sample and the duplicate is listed in the 5th column of Table 21. Then the % absorbencies of the sample and the duplicate were averaged, and the standard deviation of the average was calculated. They are listed in the 6th and 7th column of Table 21. The degelation plot was obtained by plotting the average % absorbance as a function of average temperature. The error bars represent the standard deviation.

T₅₀ was determined by drawing a line from 50% absorbance and then finding its corresponding temperature as shown in Figure 36.